AGU PUBLICATIONS

JGR

Journal of Geophysical Research: Oceans

RESEARCH ARTICLE

10.1002/2016JC012345

Variability and change of sea level and its components in the Indo-Pacific region during the altimetry era

Quran Wu[1,2], Xuebin Zhang[2], John A. Church[3], and Jianyu Hu[1]

[1]State Key Laboratory of Marine Environmental Science, College of Ocean and Earth Sciences, Xiamen University, Xiamen, China, [2]CSIRO Oceans and Atmosphere, Hobart, Tasmania, Australia, [3]Climate Change Research Centre, University of New South Wales, Sydney, New South Wales, Australia

Key Points:
- Thermosteric component dominates the interannual variability, decadal variability, and trend of the Indo-Pacific sea level
- Halosteric component is of regional importance for the decadal variability and trend of sea level in the Pacific Ocean
- Interannual and decadal variability of mass component is critical over shelf seas, but only a minor term in open oceans

Correspondence to:
X. Zhang,
xuebin.zhang@csiro.au; and
J. Hu,
hujy@xmu.edu.cn

Citation:
Wu, Q., X. Zhang, J. A. Church, and J. Hu (2017), Variability and change of sea level and its components in the Indo-Pacific region during the altimetry era, *J. Geophys. Res. Oceans*, *122*, 1862–1881, doi:10.1002/2016JC012345.

Received 19 SEP 2016
Accepted 8 FEB 2017
Accepted article online 14 FEB 2017
Published online 10 MAR 2017

Abstract Previous studies have shown that regional sea level exhibits interannual and decadal variations associated with the modes of climate variability. A better understanding of those low-frequency sea level variations benefits the detection and attribution of climate change signals. Nonetheless, the contributions of thermosteric, halosteric, and mass sea level components to sea level variability and trend patterns remain unclear. By focusing on signals associated with dominant climate modes in the Indo-Pacific region, we estimate the interannual and decadal fingerprints and trend of each sea level component utilizing a multivariate linear regression of two adjoint-based ocean reanalyses. Sea level interannual, decadal, and trend patterns primarily come from thermosteric sea level (TSSL). Halosteric sea level (HSSL) is of regional importance in the Pacific Ocean on decadal time scale and dominates sea level trends in the northeast subtropical Pacific. The compensation between TSSL and HSSL is identified in their decadal variability and trends. The interannual and decadal variability of temperature generally peak at subsurface around 100 m but that of salinity tend to be surface-intensified. Decadal temperature and salinity signals extend deeper into the ocean in some regions than their interannual equivalents. Mass sea level (MassSL) is critical for the interannual and decadal variability of sea level over shelf seas. Inconsistencies exist in MassSL trend patterns among various estimates. This study highlights regions where multiple processes work together to control sea level variability and change. Further work is required to better understand the interaction of different processes in those regions.

1. Introduction

Sea level is of great socioeconomic importance and one of the fundamental indicators for climate change. Interannual-to-decadal sea level variability is modulated by the three-dimensional redistribution of mass, heat, and salt in the ocean interior, and also by complex interactions between the ocean and other climate system components, such as the atmosphere and cryosphere [*Church et al*., 2013]. As a result, it is challenging to understand and predict sea level variability and change.

Sea level varies on broad spatial-temporal scales. For example, the global-mean sea level rose at a rate of 3.2 mm yr^{-1} over 1993–2010 [*Church et al*., 2013], while regional sea level featured trends about 10 mm yr^{-1} in the west tropical Pacific, but slightly negative values in the east tropical Pacific [e.g., *Merrifield*, 2011; *Zhang and Church*, 2012; *Stammer et al*., 2013]. The deviation of regional trend from the global-mean value is mainly due to the low-frequency variability of sea level related to various modes of climate variability, such as the El Niño Southern Oscillation (ENSO) and the Pacific Decadal Oscillation (PDO) [e.g., *Cazenave and Llovel*, 2010; *Cazenave and Remy*, 2011; *Stammer et al*., 2013]. On interannual time scale, the sea level variability associated with the ENSO is well documented in the Indo-Pacific region. During El Nino, it features anomalous sea level rises (falls) in the eastern (western) equatorial Pacific, as well as positive sea level anomalies in the western equatorial Indian Ocean [e.g., *Chambers et al*., 1999; *Nerem et al*., 1999; *Landerer et al*., 2008; *Becker et al*., 2012; *Zhang and Church*, 2012; *Chen and Wallace*, 2015; *Hamlington et al*., 2015]. On interannual-to-decadal time scales, *Zhang and Church* [2012, hereinafter ZC2012] showed that about 60% of sea level variance over the Pacific during the altimetry era can be explained by a multivariate linear regression model. The regression model used in their study considers dominant interannual and decadal climate indices and a linear trend simultaneously. The results of ZC2012 suggested that sea level trends in the

tropical Pacific are affected by the PDO-related decadal sea level variability during the altimetry era. *Bromirski et al*. [2011], *Merrifield et al*. [2012], and *Moon et al*. [2013] reached a similar conclusion and found that enhanced sea level trends in the west tropical Pacific are driven by an intensification of trade wind associated with a recent shift of the PDO. Based on the empirical orthogonal function (EOF) analysis, *Hamlington et al*. [2014] estimated the PDO contribution to sea level trends in the Pacific over 1993–2010. By removing the PDO contribution, they found 5 mm yr^{-1} sea level rises to the east of the Philippines and northeast of Australia, which they argued may be due to anthropogenic forcing. Moreover, *Moon et al*. [2015] examined the joint effect of PDO and ENSO and found that the recent amplification of decadal sea level oscillation in the tropical Pacific is the result of more frequent in-phase relationship between the PDO and ENSO.

Many efforts have been made to understand the mechanisms of sea level variability. For example, the wind-driven Rossby wave model was suggested to be a valid approximation for the midlatitude interannual-to-decadal sea level variability [*Qiu and Chen*, 2006, 2012]. The surface buoyancy forcing was found negligible in the tropical and north subtropical Pacific [*Piecuch and Ponte*, 2012; *Forget and Ponte*, 2015]. *Piecuch and Ponte* [2011] pointed out that the advection term dominates the interannual variability of steric sea level in the tropical Pacific and Indian Oceans, while the diffusion term is only comparable to the advection term in extratropical latitudes.

In addition to the temporal decomposition as introduced above, sea level can be decomposed into different components, i.e., the steric and mass components [*Gill and Niller*, 1973]. The steric sea level (SSL) component accounts for water volume changes induced by density changes only (assuming no mass changes). At the same time, a regional gain or loss of mass also causes a change in water volume and a change in sea level (referred to as MassSL). The SSL component can be further decomposed into thermosteric sea level (TSSL) and halosteric sea level (HSSL) components, corresponding to the thermal expansion and haline contraction effects, respectively. Past studies have shown that for 1993–2010, the regional trend patterns of sea level highly resembled that of SSL integrated over the upper 700 m [e.g., *Cazenave and Remy*, 2011; *Stammer et al*., 2013]. The SSL trends are mostly due to the TSSL component, while the HSSL component is found to be important in some regions and tends to compensate the TSSL trends [e.g., *Antonov et al*., 2002; *Levitus et al*., 2005; *Lombard et al*., 2009; *Durack et al*., 2014]. Similarly, patterns of interannual sea level variance are primarily determined by the TSSL component, while the HSSL and MassSL are of regional importance [*Köhl*, 2014; *Forget and Ponte*, 2015]. For instance, the variability of HSSL is comparable to that of TSSL in the west tropical Pacific and extratropical regions on interannual time scale [*Landerer et al*., 2008; *Köhl*, 2014; *Forget and Ponte*, 2015]. On decadal time scale, the HSSL variability of similar magnitude to the TSSL variability is observed in the southeast subtropical Pacific [*Nidheesh et al*., 2013]. In terms of the MassSL, recent Gravity Recovery and Climate Experiment (GRACE) satellite observations [*Chambers and Bonin*, 2012] suggest that more than 50% of interannual sea level variance in several extratropical regions and shelf seas can be explained by the variations of ocean mass [*Piecuch et al*., 2013, 2015b; *Ponte and Piecuch*, 2014; *Wang et al*., 2015].

The aforementioned studies have covered various perspectives of regional sea level variability and change. In particular, *Forget and Ponte* [2015] performed a comprehensive partition of regional sea level and concluded that the TSSL, HSSL, and MassSL are all important in controlling regional sea level variability. In this study, built upon *Forget and Ponte* [2015], we aim to assess the roles of different sea level components in shaping the interannual, decadal, and trend patterns identified in ZC2012. In order to achieve this goal, we derive sea level and its components from two adjoint-based ocean reanalyses that provide dynamically self-consistent ocean states over 1992–2011 [*Thacker and Long*, 1988]. The interannual, decadal, and trend patterns are estimated for each sea level component using the multivariate linear regression model of ZC2012. The patterns of total sea level from the ocean reanalyses are examined in sections 3 and 4, along with a comparison with the altimetry results. Next the roles of different sea level components and subsurface temperature and salinity in generating the total sea level patterns are explored in section 5. The comparison of MassSL from the GRACE observations and the ocean reanalyses is also included in that section. Summary and discussion can be found in section 6.

2. Materials and Methods

2.1. Ocean Reanalyses

The two adjoint-based ocean reanalyses used in this study is Estimating the Circulation and Climate of the Ocean (ECCO, version 4 release 2) [*Forget et al*., 2015, 2016] and Estimated State of the Global Ocean for

Climate Research (ESTOC, Ver. 02b) [*Osafune et al*., 2015]. The ECCO product is based on the Massachusetts Institute of Technology general circulation model (MITgcm) [*Marshall et al*., 1997] driven by an adjusted version of ERA-Interim atmosphere reanalysis [*Dee et al*., 2011]. It has a truly global domain, 1° zonal resolution, 1/3°-1° meridional resolution (refined near the equator), and 50 vertical levels. The ESTOC product is based on the Geophysical Fluid Dynamics Laboratory Modular Ocean Model version 3 [*Pacanowski and Griffies*, 2000], which has a 1° quasi-global setup (75°S–80°N) and 46 vertical levels. The surface boundary conditions of ESTOC come from an adjusted version of the National Center for Environmental Predication/National Center for Atmospheric Research reanalysis. Both ECCO and ESTOC assimilate observational data (e.g., Argo and altimetry data) using the whole-domain adjoint approach [*Stammer et al*., 2002]. Specifically, the atmospheric forcing, oceanic initial conditions, and subgrid parameterizations are iteratively adjusted (ESTOC does not adjust the sub-grid parameters) to minimize the misfit between model and observations. Importantly, in both studies the temporal evolutions of ocean states are strictly governed by model equations, and thus can be traced back to clearly defined physical processes. The simulation period for ECCO is 1992–2011, while the ESTOC product covers the period 1957–2011, but we only use the results over 1992–2011. Neither ECCO nor ESTOC includes a detailed representation of the freshwater flux due to the loss of mass from ice sheets and glaciers directly. Therefore, we only focus on dynamic sea level (DSL), which is defined as the regional deviation of sea level from its global mean. Removing the global mean will also attenuate regional sea level interannual or decadal variability by around 1 mm, but those effects are not significantly different from 0 (based on the regression model to be introduced in section 2.3).

2.2. Sea Level Components

By neglecting nonlinear terms, the steric, thermosteric, halosteric, and mass sea level components are calculated as

$$\mathrm{SSL}\Big|_{z_1}^{z_2} = -\int_{z_1}^{z_2} \frac{\rho(T,\ S)-\rho(T_0,\ S_0)}{\rho(T_0,\ S_0)}\,dz, \tag{1}$$

$$\mathrm{TSSL}\Big|_{z_1}^{z_2} = -\int_{z_1}^{z_2} \frac{\rho(T,S_0)-\rho(T_0,\ S_0)}{\rho(T_0,\ S_0)}\,dz, \tag{2}$$

$$\mathrm{HSSL}\Big|_{z_1}^{z_2} = -\int_{z_1}^{z_2} \frac{\rho(T_0,S)-\rho(T_0,\ S_0)}{\rho(T_0,\ S_0)}\,dz, \tag{3}$$

$$\mathrm{MassSL}=\mathrm{DSL}-\mathrm{SSL}, \tag{4}$$

where ρ, T, and S represent density, temperature, and salinity of seawater, respectively. The subscript 0 denotes values at the first time step. The 1980 UNESCO International Equation of State (IES80) is used to calculate the density. z_1 and z_2 are two depths that define the lower and upper bounds of vertical integral. Generally we set z_1 to the depth of the seafloor and z_2 to the sea surface unless otherwise specified. For the ECCO product, we use direct ocean bottom pressure outputs to calculate MassSL.

2.3. Climate Indices and Multivariate Linear Regression Model

Following the multivariate linear regression model of ZC2012, here we decompose a given time series into the interannual, decadal, and trend components by regressing it with respect to the interannual and decadal climate indices and time simultaneously. All time series in this study have the climatological seasonal cycle removed first, and then are smoothed using a 5 month running-mean filter before any further analysis. The interannual climate index (ICI) is the multivariate ENSO index (MEI, http://www.esrl.noaa.gov/psd/enso/mei/) with its 6 year low-passed component removed. The decadal climate index (DCI) is the 6 year low-passed PDO index (http://jisao.washington.edu/pdo/). The construction of ICI and DCI leads to temporal independence of them (correlation of 0.17 which is below the 95% significance level; Figure 1a), so that the regression model can clearly separate sea level variability into interannual and decadal time scales. To be specific, the temporal variability of DSL at an arbitrary position is least squares fitted according to the following equation:

$$\mathrm{DSL}=c_0+\mathrm{IFP}_{\mathrm{DSL}}\cdot\mathrm{ICI}+\mathrm{DFP}_{\mathrm{DSL}}\cdot\mathrm{DCI}+\mathrm{Trend}_{\mathrm{DSL}}\cdot t+\varepsilon, \tag{5}$$

where c_0 and ε are the intercept and uncertainty of the regression model, respectively. Regression coefficients $\mathrm{IFP}_{\mathrm{DSL}}$ and $\mathrm{DFP}_{\mathrm{DSL}}$ are referred to as DSL interannual and decadal fingerprints, respectively. They

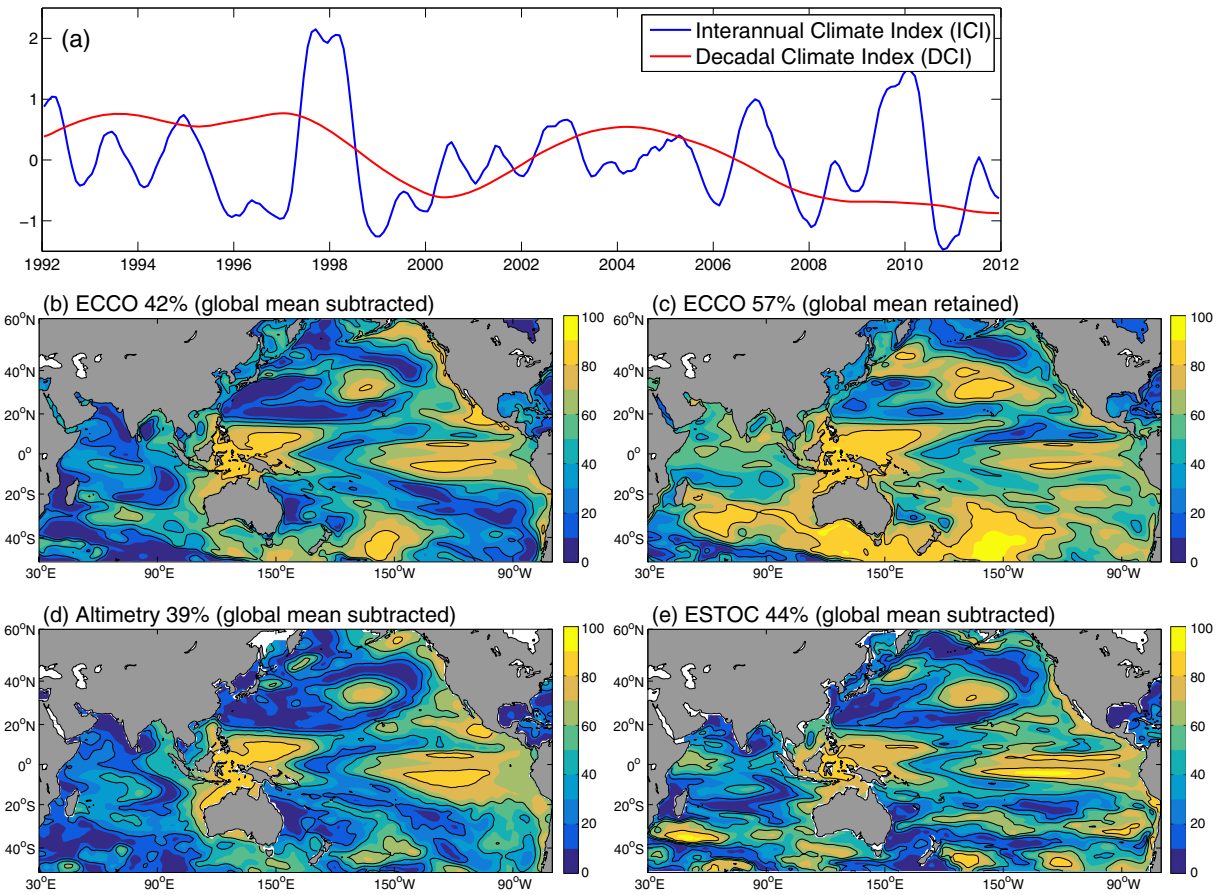

Figure 1. Interannual climate index (ICI, blue) and decadal climate index (DCI, red) used in the multivariate linear regression model (a). The percentage of sea level variance explained by the regression model (R^2) for (b, c) ECCO, (d) altimetry, and (e) ESTOC are shown for the Indo-Pacific region, with spatial means in titles. Note that the global mean sea level is retained in Figure 1c, but is removed in Figures 1b, 1d, and 1e before regression.

indicate typical magnitudes of DSL variability resolved by the regression analysis on corresponding time scales. The same regression analysis is applied to each sea level component; thus, the IFP_{DSL}, DFP_{DSL}, and $Trend_{DSL}$ can be further decomposed as

$$C_{DSL} = \overbrace{C_{TSSL} + C_{HSSL}}^{C_{SSL}} + C_{MassSL}, \quad C = \{IFP,\ DFP,\ Trend\}, \tag{6}$$

where the subscripts denote associated sea level components and C represents IFP, DFP, or trend derived from the regression model (equation (5)). These regression coefficients are used to evaluate variability and change of DSL and its components later.

The performance of a regression model is measured by the ratio between variance resolved by the regression and total variance (R^2). The R^2 value of the regression model of ZC2012 is about 40% over the Indo-Pacific region (Figure 1). Specifically, the R^2 values are about 20–40% in the Indian Ocean and are greater than 60% in the tropical Pacific, the North Pacific, and the South Pacific Subtropical Gyre. Those numbers are consistent for altimetry, ECCO, and ESTOC. Due to the simplicity of the regression model, it can only explain less than 20% of sea level variance in some extratropical regions. One may notice a drop of the R^2 value from 60% in ZC2012 to 40% in this study. This difference is primarily due to the subtraction of the global mean sea level, while the inclusion of the Indian Ocean has a smaller impact as well (compare Figure 1b with Figure 1c).

In this study, we refer to the *trend* as the regression coefficient $Trend_{DSL}$ in equation (5), and refer to the *linear trend* as the regression coefficient derived from a univariate regression with time alone as a predictor. Those two trends can be different because the decadal variability can also induce a linear trend over short

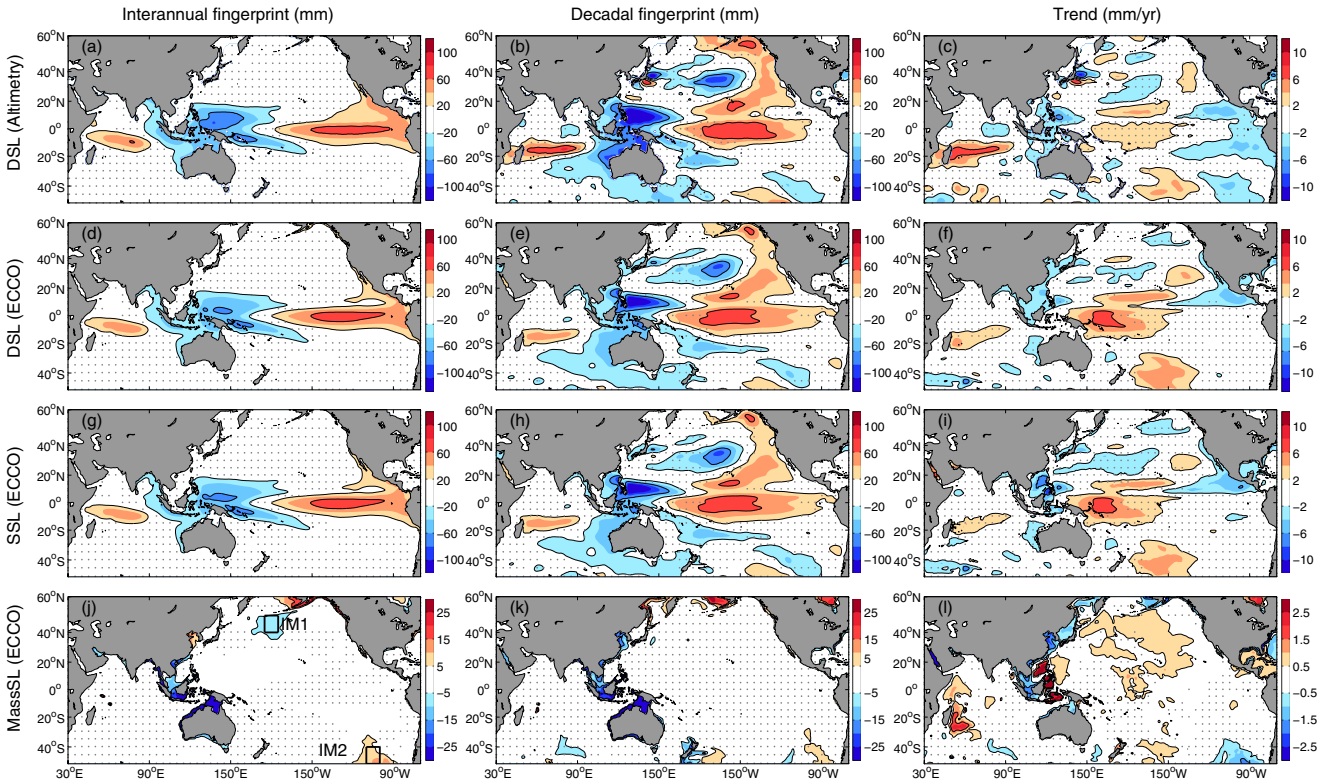

Figure 2. Interannual, decadal fingerprints, and trends of dynamic sea level (DSL), steric sea level (SSL), and mass sea level (MassSL) in the altimetry (1993–2011) and ECCO (1992–2011). Stippling denotes values below the 95% significant level. Black boxes in Figure 2j indicate regions where barotropic vorticity balance is diagnosed (see section 5.4 for the details). Note that the bottom figures have reduced color ranges.

periods. It is important to note that limited by the 20 year analysis window, the decadal fingerprints derived here may not represent their values from a long-term record (e.g., 50 year) [*Frankcombe et al.*, 2015]. The two-sided Student's *t* test is employed to identify regression coefficients that are significantly different from 0 at the 95% confidence level, using the effective degree of freedom [*Davis*, 1976; *Emery and Thomson*, 2001].

2.4. Altimetry and GRACE Observations

Monthly 1° × 1° altimetry sea level data based on merged TOPEX/Poseidon, Jason-1, and Jason-2 observations are provided by the CSIRO sea level group, corrected for both the glacial isostatic adjustment (GIA) and inverse barometer effects [*Church and White*, 2011]. The GRACE spherical harmonic solution [*Chambers and Bonin*, 2012] and mass concentration (mascon) solution [*Watkins et al.*, 2015; *Save et al.*, 2016] are used here to estimate MassSL. For the GRACE harmonic solution, we average monthly 1° × 1° data from the Center for Space Research (CSR), GeoForschungsZentrum (GFZ), and Jet Propulsion Laboratory (JPL). For the GRACE mascon solution, we use monthly 1° × 1° mascon provided by CSR [*Save et al.*, 2016]. GIA is removed from both GRACE solutions. The land leakage correction, a destriping filter, and a 500 km Gaussian filter are applied to the GRACE harmonic solution to reduce the misfit between it and in situ data (refer to *Chambers and Bonin* [2012], *Watkins et al.* [2015], *Save et al.* [2016], and http://grace.jpl.nasa.gov for more information about the GRACE data processing).

3. Validation of ECCO and ESTOC Results

The interannual, decadal, and trend maps of DSL (i.e., IFP_{DSL}, DFP_{DSL}, and $Trend_{DSL}$) derived from altimetry are compared with those from ECCO and ESTOC to evaluate the performance of the two reanalyses in reproducing observed DSL signals. The map of IFP_{DSL} is similar for all the three data sets (Figures 2a, 2d, and 3d), with spatial correlations of more than 0.95 among them (Table 1). Such similarity can also be found among DFP_{DSL} maps (Figures 2b, 2e, and 3e). The maps of $Trend_{DSL}$ (Figures 2c, 2f, and 3f), however, are

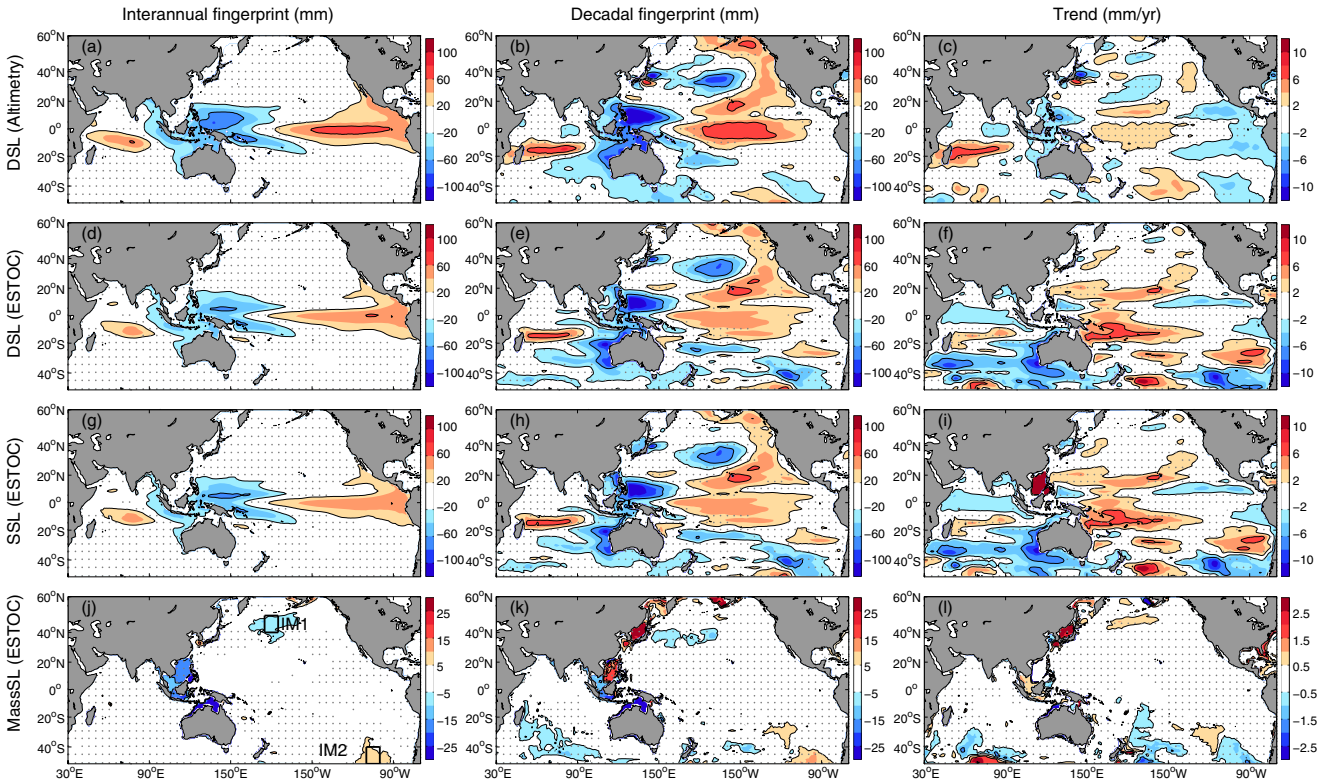

Figure 3. Same as Figure 2, but for ESTOC.

less consistent, as the spatial correlations among them drop to 0.4–0.7 (Table 1). Despite being driven by different atmospheric forcing, both ECCO and ESTOC overestimate trends in the west tropical Pacific and the South Pacific Subtropical Gyre, underestimate trends in the southwest tropical Indian Ocean, and fail to capture negative trends in the east tropical and far southeast Pacific. ECCO has better performance than ESTOC in replicating the observed DSL signals (Table 1). For example, the IFP_{DSL} and DFP_{DSL} derived from ESTOC are weaker than those from either the altimetry or ECCO in the tropical Pacific (Figures 2a, 2b, 2d, 2e, 3d, and 3e). In the south subtropical Indo-Pacific region and the Southern Ocean (SO), the trend differences between ESTOC and altimetry could reach 4 mm yr^{-1} (Figures 3c and 3f). The lower agreement between ESTOC and altimetry is, to some degree, not surprising given the fact that ESTOC is optimized to reduce model-data misfits over a 55 year period (1957–2011), rather than for the altimetry era only as in ECCO.

Based on the comparisons presented here, we conclude that ECCO and ESTOC are capable of reproducing much of observed DSL fingerprints and some of DSL trends in the Indo-Pacific region, justifying our further decomposition of DSL from these two data sets. In the following discussions, we focus on robust patterns across ECCO and ESTOC. But in the south subtropical Indo-Pacific region and the SO, only ECCO results are considered. This is because of the questionable trends of ESTOC in these regions (Figure 3f).

Table 1. Spatial Correlation Coefficients of Interannual, Decadal, and Trend Patterns of Dynamic Sea Level Among Altimetry, ECCO, and ESTOC, Over the Indo-Pacific Region (30°E–70°W, 50°S–60°N)[a]

	ECCO Versus Altimetry	ESTOC Versus Altimetry	ECCO Versus ESTOC
Interannual	0.98 ± 0.01	0.95 ± 0.02	0.97 ± 0.01
Decadal	0.95 ± 0.02	0.87 ± 0.04	0.88 ± 0.04
Trend	0.69 ± 0.07	0.41 ± 0.11	0.51 ± 0.10

[a]Error bars denote the 95% confidence intervals based on 1000 bootstrap samples.

4. Interannual, Decadal Fingerprints, and Trends of DSL

The interannual fingerprint of DSL (IFP_{DSL}) exhibits a seesaw pattern in the tropical Pacific, and zonally elongated positive anomalies in the southwest tropical Indian Ocean (Figures 2d and 3d). The maximum magnitudes are on the equator in the eastern Pacific (60–80 mm), but slightly off the equator in the western Pacific (60–80 mm) and the Indian Ocean (40–60 mm). There are also weak (20–40 mm) but significant values of IFP_{DSL} found along the coastal waveguides in the eastern Indian and Pacific Oceans. These patterns are consistent with previous studies using alternative approaches [e.g., *Nerem et al*., 1999; *Landerer et al*., 2008]. In the tropical Pacific, the IFP_{DSL} can be explained by the zonal heat content redistribution and equatorial waves associated with ENSO events [*Enfield and Allen*, 1980; *Jin*, 1997; *Meinen and McPhaden*, 2000; *Wijffels and Meyers*, 2004]. In the Indian Ocean, the westward propagation of thermocline anomalies from the west tropical Pacific may be responsible for the IFP_{DSL} found there [*Feng and Meyers*, 2003; *Wijffels and Meyers*, 2004; *Cai*, 2005; *Schwarzkopf and Böning*, 2011; *Trenary and Han*, 2012]. Note that the lack of IFP_{DSL} in midlatitudes does not necessarily indicate that there is no interannual DSL variability, since the variability unrelated to the ICI (interannual climate index) cannot be resolved by the regression model of ZC2012, as discussed in section 2.3.

Compared to the IFP_{DSL}, the decadal fingerprint of DSL (DFP_{DSL}) extends to the mid and highlatitudes (Figures 2e and 3e), consistent with the broad meridional distribution of the PDO patterns [e.g., *Mantua and Hare*, 2002; *Deser et al*., 2010]. Due to the temporal decorrelation of ICI and DCI, the spatial correlation between IFP_{DSL} and DFP_{DSL} is rather low at 0.52 ± 0.12. In the North Pacific, the DFP_{DSL} shows negative anomalies with the minimums centered at 170°W, 34°N, surrounded by horseshoe shape positive anomalies (20–60 mm; Figures 2e and 3e). These anomalies extend from the US West Coast to the equatorial Pacific and are close to the pathway of the Pacific shallow overturning circulation [*McCreary and Lu*, 1994]. Similar decadal sea level variability patterns can be derived by regressing sea level onto the Interdecadal Pacific Oscillation (IPO) index using observational or model data [*Lyu et al*., 2015]. In the North Pacific, enhanced negative DFP_{DSL} (centered at 170°W, 34°N) was hypothesized to be associated with the cyclonic wind stress anomalies during the positive PDO phase in past studies [e.g., *Moon et al*., 2013; *Lyu et al*., 2015]. The elevated decadal variability in the southwest tropical Indian Ocean is also presented in *Li and Han* [2015]'s 50 year numerical simulation driven by decadal fluctuations of wind stress. The coherent DFP_{DSL} extending from the west tropical Pacific to the South Indian Ocean through the eastern boundary waveguides in part reflect the oceanic connection of decadal sea level variability between those two basins [*Feng*, 2004; *Lee and McPhaden*, 2008; *Feng et al*., 2010, 2011; *Schwarzkopf and Böning*, 2011].

DSL rises larger than 2 mm yr^{-1} are found in the northeast subtropical Pacific, the west tropical Pacific, the South Pacific Subtropical Gyre, and the southwest tropical Indian Ocean (Figures 2c, 2f, and 3f). In contrast, DSL falls around -2 mm yr^{-1} are evident in the east tropical Pacific, the far southeast Pacific, and the North Pacific (centered at 180°E, 25°N) in altimetry (Figure 2c). But they are only partially reproduced by ECCO and ESTOC (Figures 2f and 3f). Limited by 20 year data and possibly other decadal-to-multidecadal climate modes that are not represented in our regression model, we should not assume that those trends are purely due to climate change (ZC2012). The positive DSL trends in the South Pacific Subtropical Gyre can also be inferred from enhanced heat gains of 5–10 W m^{-2} over 2006–2013 in that region [*Roemmich et al*., 2015] and could be a response to both wind and buoyancy forcing [*Forget and Ponte*, 2015; *Zhang and Qu*, 2015; *Roemmich et al*., 2016]. In addition, the positive DFP_{DSL} in the southwest tropical Indian Ocean implies negative linear trends over 1992–2011 (refer to the negative linear trend of DCI in Figure 1a) and tend to suppress the collocated DSL rises.

5. Contributions of Sea Level Components to the DSL Variability and Change

The roles of different sea level components in shaping the DSL patterns (i.e., Figures 2d–2f and 3d–3f) are examined in this section. By doing so, the interannual, decadal fingerprints, and trends of DSL (IFP_{DSL}, DFP_{DSL}, and $Trend_{DSL}$) are decomposed into the SSL (TSSL and HSSL) and MassSL components (equation (6)). The DSL patterns are largely determined by the SSL component (compare Figures 2d–2f with Figures 2g–2i and similarly for Figure 3), and primarily due to its TSSL component (compare Figures 2g–2i with Figures 4a–4c, and Figures 3g–3i with Figures 5a–5c). The crucial role of TSSL in controlling DSL variability and

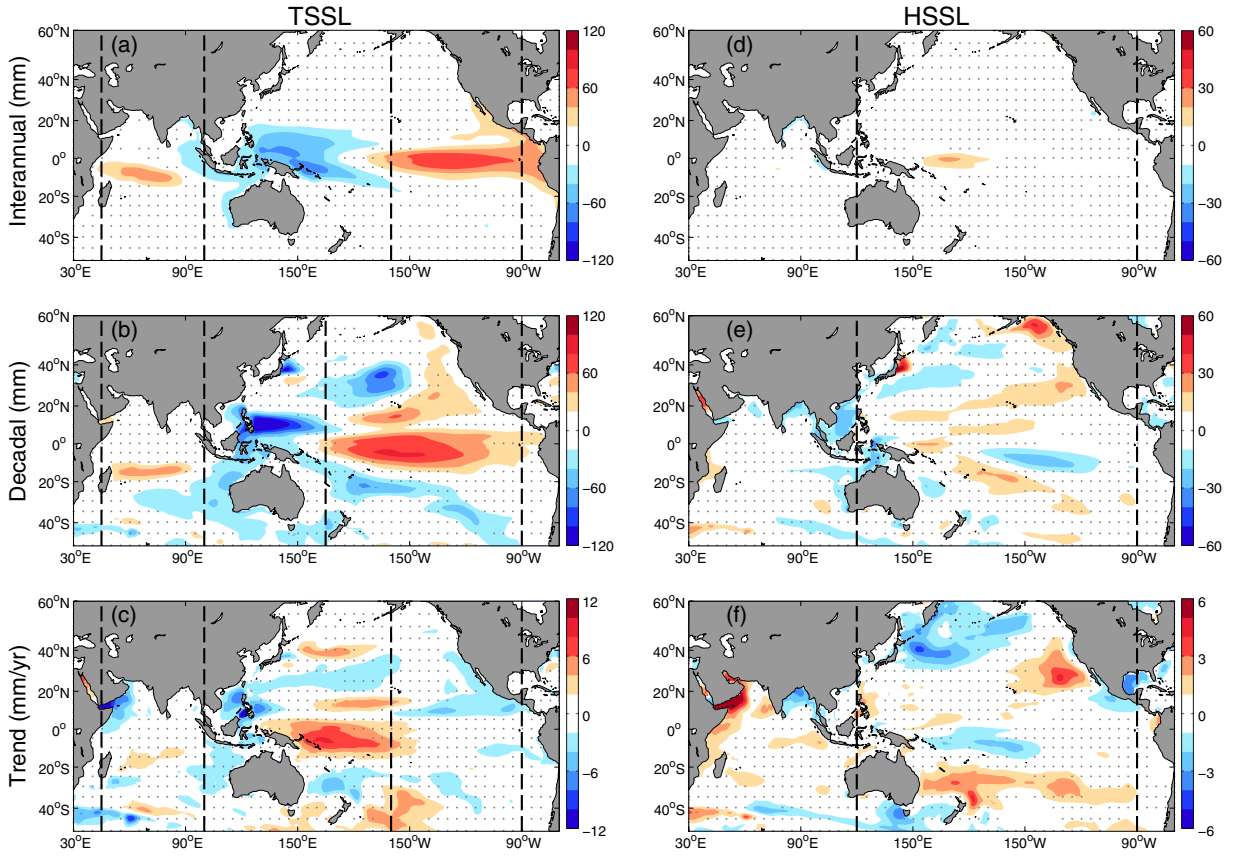

Figure 4. Interannual, decadal fingerprints, and trends of thermosteric sea level (TSSL, left) and halosteric sea level (HSSL, right) in ECCO. Values not significant at the 95% level are stippled. Black dash lines are used to separate the Indo-Pacific region into several longitude bands (see section 5.2 for the details). Note that right figures have reduced color ranges.

change found in this study agrees with *Stammer et al.* [2013], *Köhl* [2014], and *Forget and Ponte* [2015]. Nonetheless, there are also significant HSSL and MassSL fingerprints and trend that cannot be neglected in some regions, as suggested in *Forget and Ponte* [2015]. To compare regional importance of different sea level components, in particular for HSSL and MassSL, we calculate their percentage variance relative to DSL variance. The percentage variance of IFP_{TSSL}, DFP_{TSSL}, and $Trend_{TSSL}$ are defined as

$$PVAR(IFP_{TSSL}) = \frac{VAR(ICI \cdot IFP_{TSSL})}{VAR(DSL)}, \tag{7}$$

$$PVAR(DFP_{TSSL}) = \frac{VAR(DCI \cdot DFP_{TSSL})}{VAR(DSL)}, \tag{8}$$

$$PVAR(Trend_{TSSL}) = \frac{VAR(t \cdot Trend_{TSSL})}{VAR(DSL)}, \tag{9}$$

where VAR () is a function to calculate variance. The percentage variance of HSSL and MassSL are calculated in the same manner. Because of the compensation between different sea level components on the same time scale (e.g., $Trend_{HSSL}$ and $Trend_{TSSL}$) or between sea level variations on different time scales (e.g., $DCI \cdot DFP_{DSL}$ and $t \cdot Trend_{DSL}$), the percentage variance could be greater than 1 in some regions (e.g., purple regions in Figures 6 and 7).

5.1. The Role of HSSL

The interannual fingerprint of HSSL (IFP_{HSSL}) with magnitudes of 10–30 mm are observed in the western equatorial Pacific (Figures 4d and 5d), accounting for about 10–20% of DSL variance (Figures 6g and 7g). Apart from that, the IFP_{HSSL} is mostly negligible in the Indo-Pacific region. The decadal fingerprint of HSSL (DFP_{HSSL}) is visible in a broad region of the Pacific Ocean with magnitudes of 10–20 mm (Figures 4e and

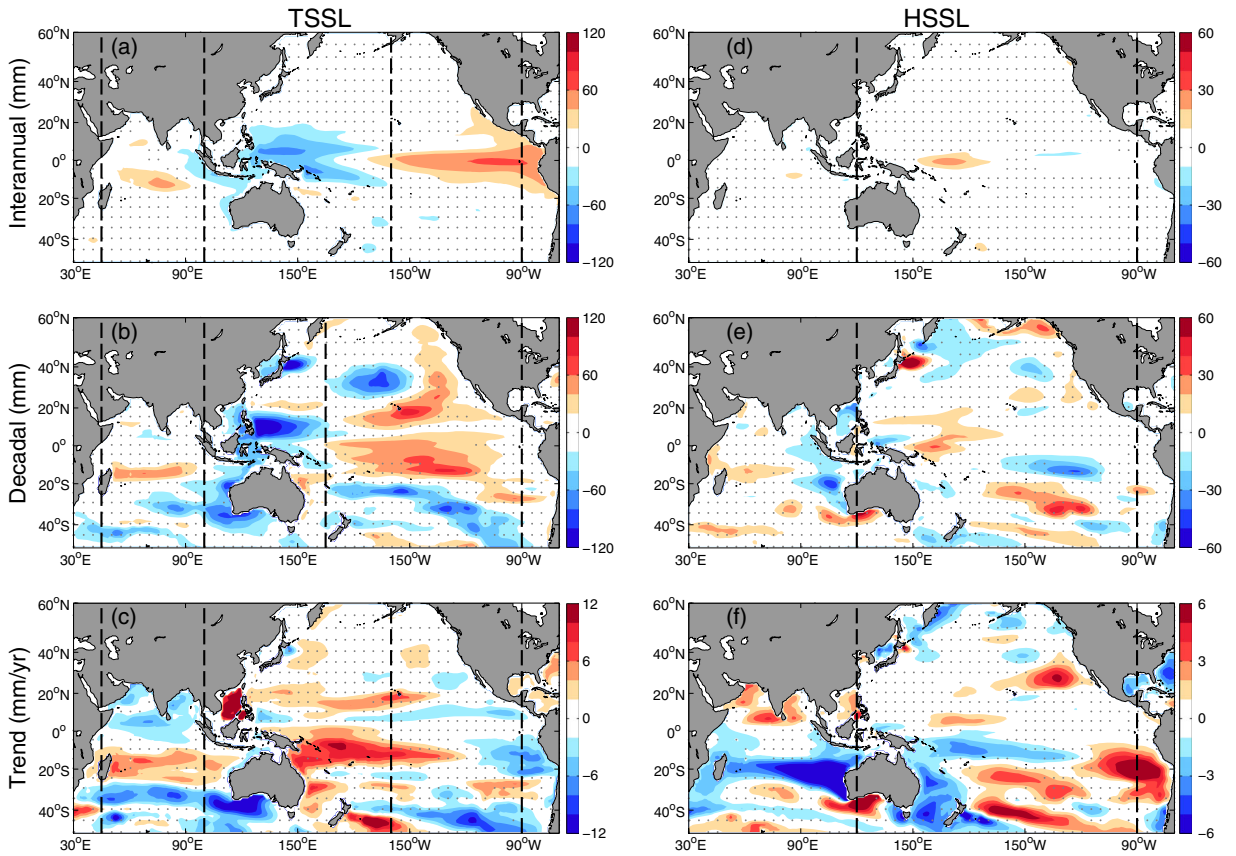

Figure 5. Same as Figure 4, but for ESTOC.

5e). Around 10–20% of DSL variance can be explained by the DFP_{HSSL} in the south tropical Pacific, the subtropical Pacific, and offshore the US west coast (some may reach 40% in ESTOC; Figures 6h and 7h). In the Indian Ocean, the DFP_{HSSL} is weak in the basin interior, but significant signals are observed off West Australia and near the SO, with magnitudes about 10 mm (Figures 4e and 5e). The significant DFP_{HSSL} in the Pacific tend to compensate the DFP_{TSSL} (black contours in Figures 6h and 7h), except offshore the US west coast where the two components work in concert (outside black contours in Figures 6h and 7h). Both ECCO and ESTOC feature HSSL trends about $+3$ mm yr^{-1} in the northeast subtropical Pacific, and about -2 mm yr^{-1} trends in the western equatorial Pacific (Figures 4f and 5f). Importantly, the HSSL trends in the northeast subtropical Pacific account for more than 40% of DSL variance there and are an important part of the DSL trends in that region. In addition, ECCO alone exhibits HSSL trends about -2 mm yr^{-1} in the far northwest Pacific, and around $+2$ mm yr^{-1} HSSL trends in the south subtropical Pacific. Those HSSL trends explain 20–40% of local DSL variance, and tend to counteract the TSSL trends there (Figure 6i).

The positive IFP_{HSSL} found in the western equatorial Pacific (Figures 4d and 5d) are consistent with the freshening of the surface ocean during El Niño events [*Delcroix and Hénin*, 1991; *Delcroix and McPhaden*, 2002; *Roemmich and Gilson*, 2011]. On longer time scales, *Zhang and Qu* [2014, 2015] reported a decadal decrease of sea surface salinity in the south tropical Pacific from Argo during 2004–2012, which favors a decadal increase of HSSL in that region. *Llovel and Lee* [2015] identified 4+ mm yr^{-1} HSSL rises over 2005–2013 in the southeast tropical Indian Ocean using Argo data. Those two phenomena are absent in the HSSL trend maps (Figures 4f and 5f) of our 20 year analysis, but they appear in the decadal HSSL maps (Figures 4e and 5e). To be specific, regressed decadal HSSL (i.e., $DCI{\cdot}DFP_{HSSL}$) in ECCO are equivalent to about 2 mm yr^{-1} HSSL rises in the southeast tropical Indian Ocean, and about 4 mm yr^{-1} HSSL rises in the south tropical Pacific over 2004–2011. The important role of HSSL in the long-term change of SSL is also reported by *Durack et al.* [2014] in the subtropical Pacific.

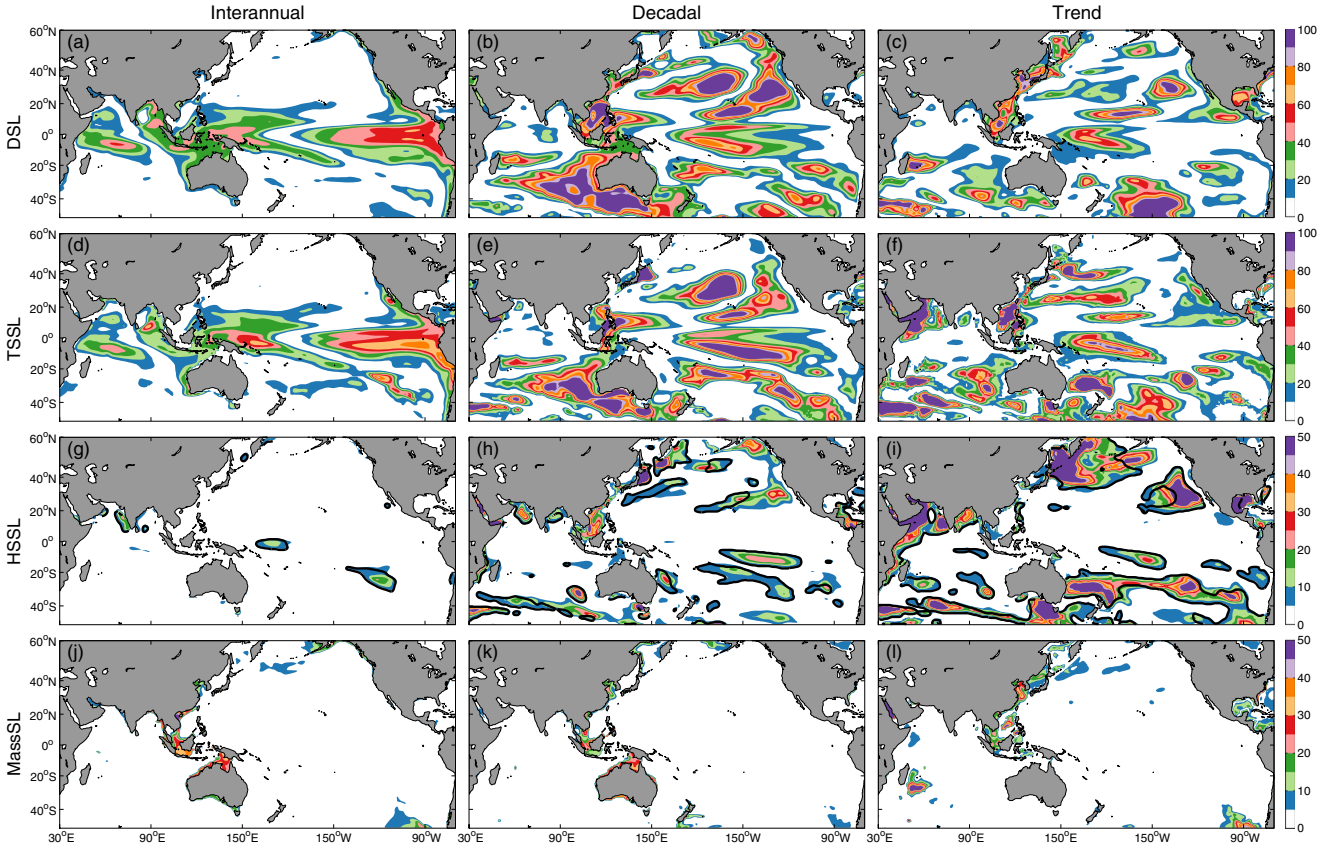

Figure 6. Fractional variance of various regressed sea level components relative to DSL total variance (based on equations (7)–(9)) in ECCO. Maps of regressed DSL, TSSL, HSSL, and MassSL are shown in the first to fourth rows, respectively. Maps on different time scales are presented in different columns. Note that the third and fourth rows have reduced color ranges. In maps of HSSL (g–i), black contours indicate regions where fingerprints or trends of TSSL and HSSL have different signs (i.e., compensating each other).

5.2. Subsurface Temperature and Salinity Responses

The variability and change of subsurface temperature and salinity that shape the TSSL and HSSL signals are also explored. The regression model of ZC2012 is applied to the temperature and salinity fields to derive their interannual and decadal fingerprints and trend. Those results are then zonal-averaged and shown as a function of depth and latitude. To avoid the cancellations of temperature fingerprints or trend after a zonal average, we divide the Indo-Pacific region into three sections, i.e., the Indian Ocean (45°E–100°E), the West Pacific Ocean (100°E–160°W), and the East Pacific Ocean (160°W–90°W). For the decadal fingerprint, the longitude that separates the West and East Pacific is modified from 160°W to 165°E so as not to break the large-scale decadal patterns during the zonal average (Figures 4b and 5b). The fingerprints and trend of salinity are averaged in the same manner but for the Pacific Ocean (120°E–90°W) only, since the HSSL fingerprints and trends are weak in the Indian Ocean. These longitude bands are denoted by black dash lines in Figures 4 and 5.

ECCO and ESTOC exhibit consistent subsurface patterns of the interannual and decadal temperature fingerprints, especially in the tropics (Figures 8 and 9). Those temperature fingerprints tend to peak at around 100 m depth in the tropics, while surface intensified signals are observed in some extratropical regions on decadal time scale, especially for ESTOC. The collocation of subsurface peaks and local thermocline depths suggests that the thermocline movement plays a role in controlling TSSL variability, in agreement with *Köhl* [2014] and *Palanisamy et al*. [2015b]. Compared to the interannual signals, the decadal signals have a broader meridional extent and are able to penetrate into greater depths in some regions, e.g., near 15°S of the Indian Ocean (Figures 8b and 9b) and around 15°N of the West Pacific Ocean (Figures 8e and 9e). The similarity of temperature trends is less than that of temperature fingerprints between ECCO and ESTOC, particularly in the subtropical South Indo-Pacific region and the SO where ESTOC displays questionable DSL trends (Figure 3f). Apart from the

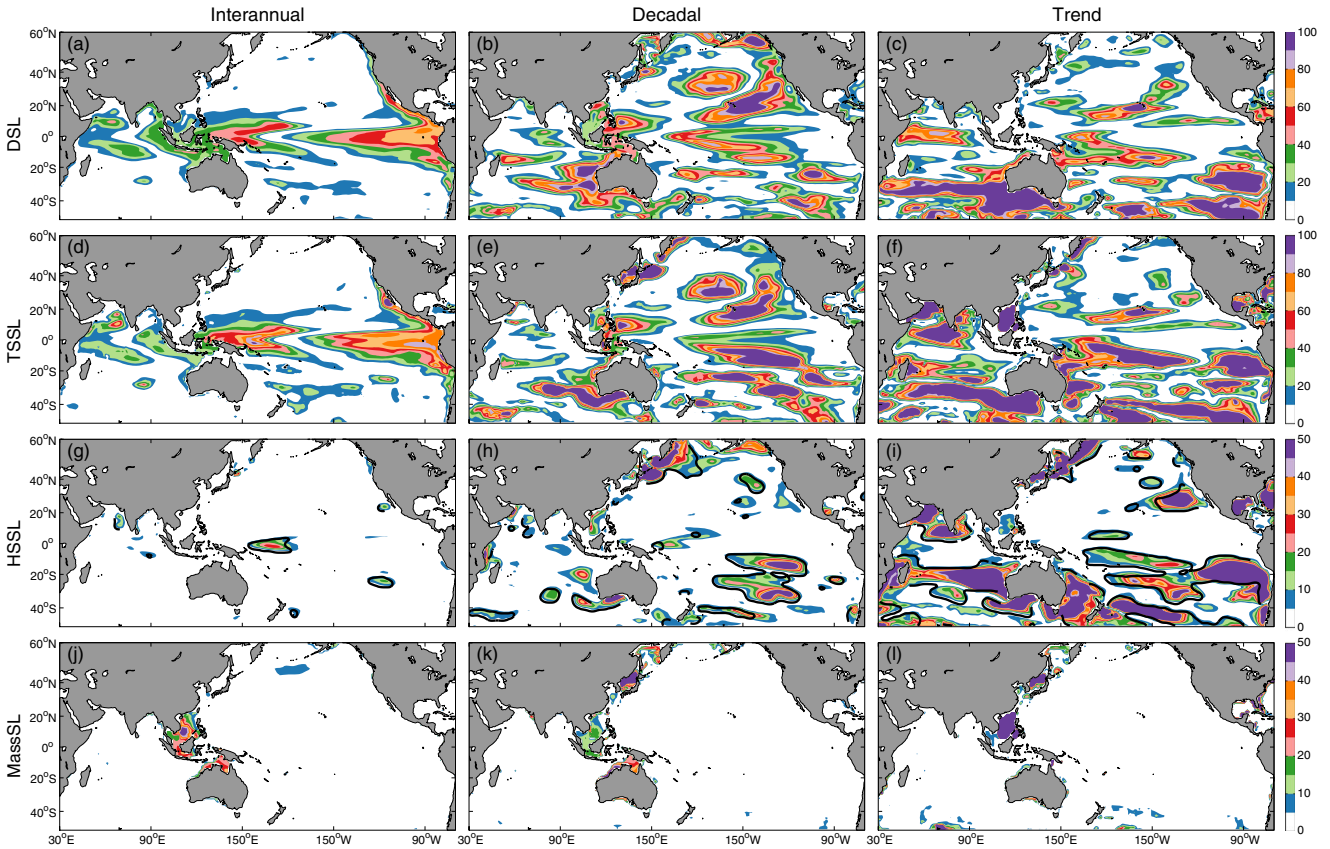

Figure 7. Same as Figure 6, but for ESTOC.

discrepancies, the subsurface temperature trends are similar for ECCO and ESTOC in the western tropical Pacific (Figures 8f and 9f).

Consistent subsurface patterns are found for the interannual and decadal fingerprints of salinity in the Pacific Ocean between ECCO and ESTOC (Figure 10). Unlike the temperature fingerprints, the salinity fingerprints tend to be surface intensified, suggesting that the freshwater forcing plays a key role in the HSSL variability. The deeper extents of decadal signals relative to interannual signals are also apparent for salinity. The freshening of upper 200–400 m water column in the subtropical Pacific is observed in ECCO (Figure 10c), resulting in 2–3 mm yr^{-1} HSSL rises over there (Figure 4f). Similar phenomenon can be found for ESTOC around 30°N (Figures 5f and 10f). In addition, the -2 mm yr^{-1} HSSL trends in the western tropical Pacific (Figures 4f and 5f) have different subsurface expressions in ECCO and ESTOC. The core of the salinity trends (near 10°S) is at the 200 m depth for ECCO, but at the surface for ESTOC (Figures 10c and 10f).

5.3. The Role of MassSL

The interannual and decadal fingerprints of MassSL are primarily confined around Australia and on the shelves of the Java Sea, the South China Sea, and the East China Sea, with magnitudes about 20–40 mm (Figures 2j, 2k, 3j, and 3k). These MassSL fingerprints account for 20–30% of DSL variance on both interannual and decadal time scales (Figures 6j, 6k, 7j, and 7k), which surpasses the roles of TSSL and HSSL in those regions. In the open oceans, the MassSL fingerprint with magnitudes larger than 5 mm can only be found in the far North and Southeast Pacific Ocean on interannual time scale (Figures 2j and 3j). They are responsible for 5–10% of DSL variance in limited regions (Figures 6j and 7j). On decadal time scale, the significant signals of MassSL fingerprint are observed in some extratropical regions (Figures 2k and 3k), but less than 5% of DSL variance can be explained by them (Figures 6k and 7k). In addition, there are large differences in MassSL fingerprints between ECCO and ESTOC in the Asian marginal seas. Magnitudes of MassSL trends are generally smaller than 0.5 mm yr^{-1} (Figures 2l and 3l). These values are negligible compared to the TSSL or HSSL trends in most of the Indo-Pacific region. One prominent feature of the ECCO results is the

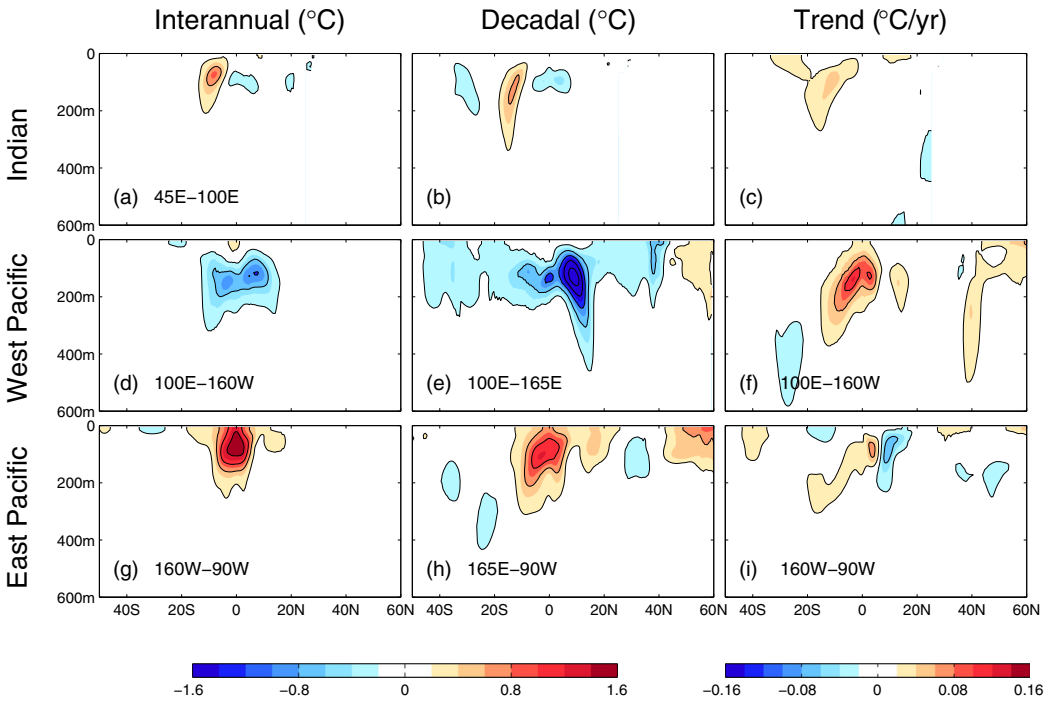

Figure 8. Interannual, decadal fingerprints, and trends of temperature averaged over the Indian Ocean (45°E–100°E) and the Pacific Ocean (100°E–90°W) from ECCO, shown as a function of depth and latitude. The West and East Pacific are separated at 160°W for the interannual fingerprints and trends, but at 165°E for the decadal fingerprints (illustrated using black dash lines in Figures 4). Contour intervals are 0.4°C and 0.04°C/yr for fingerprints and trends, respectively.

accumulation of mass (around 2 mm yr^{-1}) in deep basins (depth >3000 m) of the West Indian Ocean, the South China Sea, and the Java Sea. ECCO also features 1–2 mm yr^{-1} mass losses on the shelves of the Asian marginal seas. However, these trend patterns cannot be found in ESTOC.

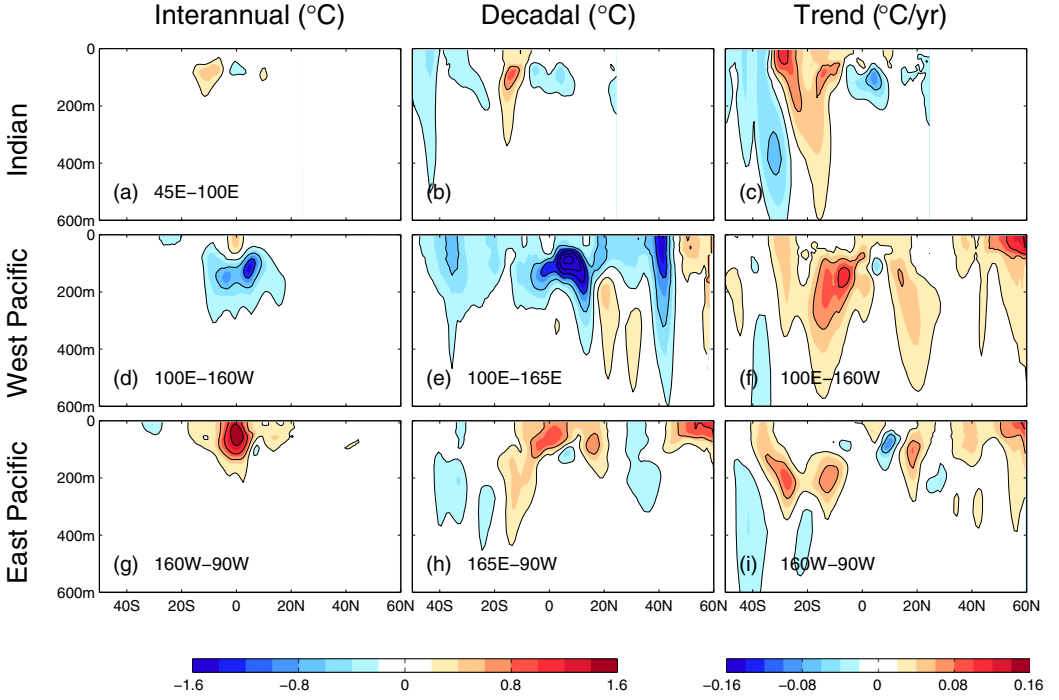

Figure 9. Same as Figure 8, but derived from ESTOC.

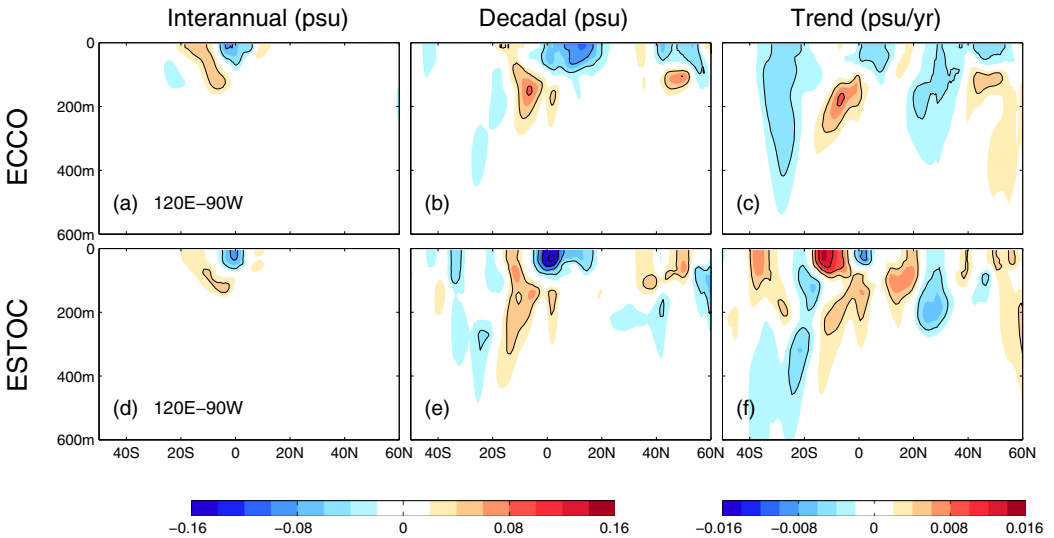

Figure 10. Interannual, decadal fingerprints, and trends of salinity averaged over the Pacific Ocean (120°E–90°W) shown as a function of depth and latitude from (a–c) ECCO and (d–f) ESTOC. (a, b, d, e) The contour intervals is 0.04 psu starting from 0 for the fingerprints. (c, f) The interval changes to 0.004 psu/yr for the trends.

Different from DSL and SSL, MassSL is not directly constrained by observations in either ECCO or ESTOC and may be affected by the accumulation of simulation errors from the other sea level components. In an attempt to assess the performance of ECCO and ESTOC in representing MassSL, we compare the model derived MassSL with the GRACE observations. The global mean is removed for all the GRACE data to reveal the regional redistribution of ocean mass, as well as to remove the effect of atmospheric pressure that is not included in ECCO and ESTOC [*Forget and Ponte*, 2015; *Osafune et al*., 2015]. The detrended, nonseasonal standard deviation and the linear trend of MassSL are calculated for 2003–2011 using the GRACE harmonic solution, the GRACE mascon solution, as well as the ECCO and ESTOC outputs, with the global means removed for all the data sets. The local maximums of standard deviation are found in the far North Pacific, the Southeast Pacific sector of the SO, and the Indian Ocean sector of the SO for all the data sets (Figures 11a–11d). In particular, there is a good agreement of the standard deviation maps among the GRACE mascon, ECCO, and ESTOC, in terms of both magnitudes and spatial patterns. Compared to the other data sets, the standard deviation of the GRACE harmonic solution is stronger in the tropics, but weaker in the highlatitudes. This could be a result of high noise level (standard error at 1–2 cm) and large-scale spatial filters applied to the GRACE harmonic solution [*Chambers and Bonin*, 2012].

In the maps of linear trend, the GRACE harmonic and mascon solutions both illustrate hemispherically asymmetric patterns in the Pacific Ocean, with around 2–3 mm yr^{-1} MassSL rises in the North Pacific, and a similar rate of MassSL falls in the South Pacific (Figures 11e–11h). Compared to that, the ECCO and ESTOC results are a factor of 2 smaller in the North Pacific and show insignificant linear trends in the South Pacific. In the Southeast Pacific sector of the SO, coherent MassSL linear trends are observed with similar shapes in the GRACE mascon and the two ocean reanalyses, but they appear to be distorted in the GRACE harmonic solution, possibly as a result of the contamination of land signals from Antarctica. The magnitudes of that linear trend patterns, however, are less consistent among different data sets. In the East Indian Ocean, the GRACE signals are dominated by negative linear trends greater than 3 mm yr^{-1} in low latitudes, which are possibly affected by a local earthquake in 2004 [*Johnson and Chambers*, 2013]. In addition, ESTOC exhibits negative linear trends over 2003–2011 with magnitudes greater than 5 mm yr^{-1} in the South China Sea and the Japan Sea. But this phenomenon cannot be observed in other data sets (Figures 11e–11h). This could reflect that ESTOC might not fully resolve key processes in marginal seas and needs further investigation.

5.4. Mechanisms of MassSL Variability

It has been suggested that different processes control the variability of MassSL in the shelf seas and the open oceans. On one hand, the prominent convergence or divergence of ocean mass around Australia can be explained as a passive response to the adjacent SSL changes (with fingerprints at 20–60 mm, Figures 2g,

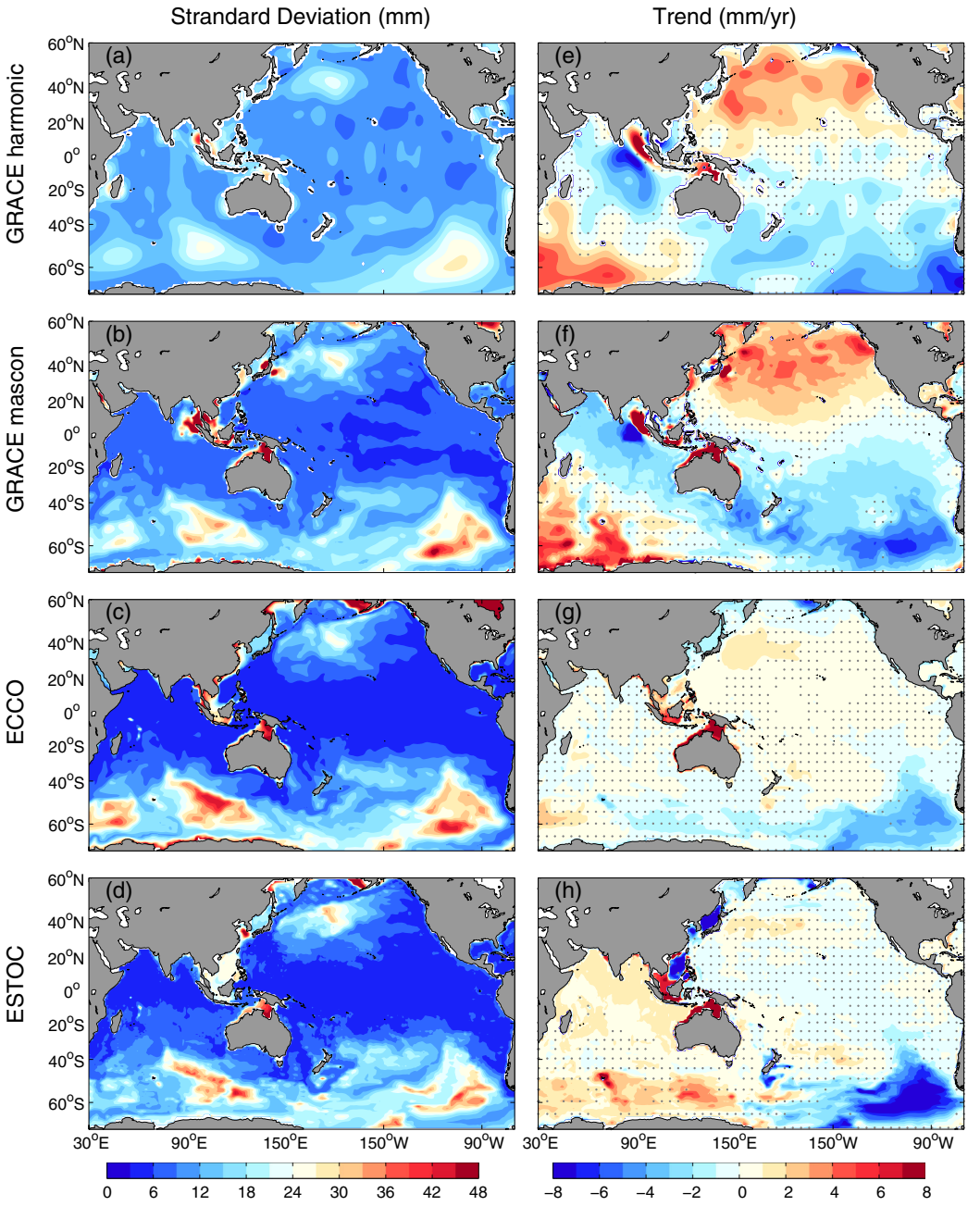

Figure 11. Nonseasonal standard deviation (left column) and linear trends (right column) of MassSL over 2003–2011 based on (a, e) GRACE spherical harmonic solution, (b, f) GRACE mass concentration solution (mascon), (c, g) ECCO, and (d, h) ESTOC. The global mean MassSL is subtracted from all data sets before calculations. For the linear trends, values not significant at the 95% level are stippled.

2h, 3g, and 3h) via the pressure gradient force [*Wang et al.*, 2015]. On the other hand, several papers argued that the interannual variability of MassSL in highlatitudes appears modulated by local wind stress curl changes [e.g., *Boening et al.*, 2011; *Ponte and Piecuch*, 2014]. Those wind stress curl changes could be further linked to ENSO events [*Song and Zlotnicki*, 2008; *Chambers*, 2011]. To investigate if such dynamics plays a role in generating the MassSL interannual fingerprints observed in the open oceans (Figures 2j and 3j), we diagnose the barotropic vorticity balance in the far North and Southeast Pacific following *Boening et al.* [2011]. After neglecting the baroclinicity, atmospheric pressure, and damping effects, the barotropic vorticity equation is

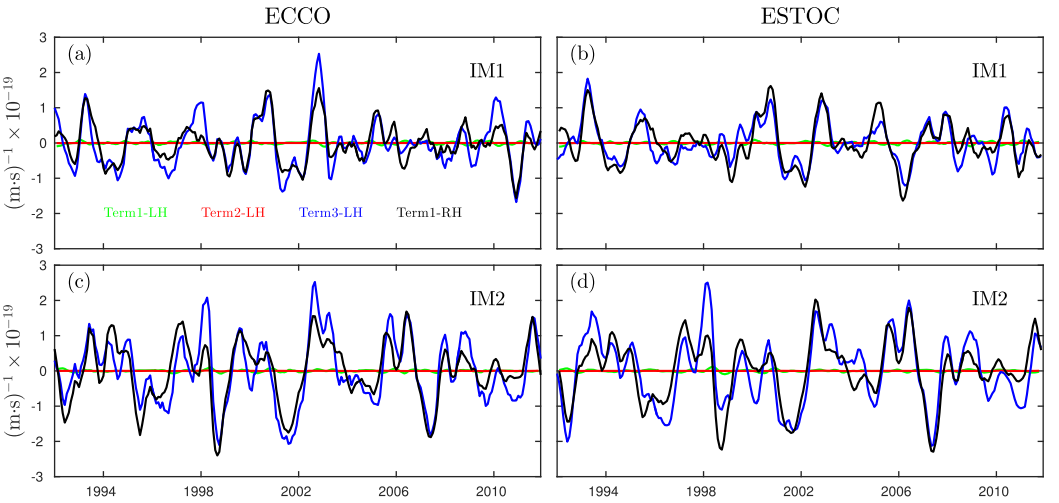

Figure 12. Box-averaged terms of the barotropic vorticity equation (equation (10)) derived from (a, c) ECCO and (b, d) ESTOC on interannual time scale. The top and bottom figures show results averaged over boxes IM1 and IM2, respectively. The positions of IM1 and IM2 are labeled in Figures 2j and 3j.

$$\frac{\partial}{\partial t}\nabla^2\eta - \frac{f^2}{gH}\frac{\partial \eta}{\partial t} + HJ\left(\eta, \frac{f}{H}\right) = \frac{f}{\rho g}\nabla \times \frac{\tau}{H}, \tag{10}$$

where J denotes the Jacobian operator, η the barotropic sea level (i.e., MassSL in this study), f the Coriolis parameter, H ocean depth, τ wind stress, g the acceleration of gravity, and ρ is ocean density. The three terms in the left-hand side of the equation (10) represent the vorticity tendency due to changes in the relative vorticity (Term1-LH), the stretching of water column (Term2-LH), and the geostrophic advection of the planetary vorticity (Term3-LH), while the right-hand side term (Term1-RH) represents the vorticity input through wind stress curl. The seasonal cycle and the 6 year low-passed component are removed from the ECCO and ESTOC outputs, before calculating each term in equation (10). Results are averaged over the boxes IM1 and IM2 (labeled in Figures 2j and 3j) representing the hot spots of MassSL interannual fingerprints in the open oceans. In both IM1 and IM2, the dominant terms of equation (10) are Term3-LH (the geostrophic advection of the planetary vorticity) and Term1-RH (the vorticity input due to the wind stress curl), and they largely balance each other (Figure 12). This implies that local wind stress curl plays an important role in modulating the interannual variability of MassSL. This result is consistent with *Boening et al.* [2011] who performed a similar analysis but based on observations over 2007–2009 in the far southeast Pacific.

Equation (10) is also diagnosed with the 6 year low-passed outputs of ECCO and ESTOC. In this case, equation (10) is not balanced (not shown), suggesting that for longer time scales (periods $>$ 6 years), the barotropic vorticity model is not a valid approximation. This result is different from *Cheng et al.* [2013] who argued that the MassSL rise in the North Pacific is driven by wind stress curl change over 2003–2011, but is consistent with *Ponte and Piecuch* [2014] and *Piecuch et al.* [2015b] who found that the baroclinic terms become nonnegligible in controlling MassSL on the time scale of a few years.

6. Summary and Discussion

In this study, we have assessed the roles of various sea level components in generating the DSL interannual, decadal, and trend patterns in the Indo-Pacific region. Sea level and its components are calculated from two adjoint-based ocean reanalyses, ECCO, and ESTOC, with the global mean removed. The interannual, decadal, and trend patterns are extracted using the regression model of ZC2012.

We find that the DSL interannual, decadal, and trend patterns are to the first order determined by TSSL in the Indo-Pacific region, consistent with *Stammer et al.* [2013], *Köhl* [2014], and *Forget and Ponte* [2015]. The interannual HSSL patterns are weak and account for less than 5% of DSL variance in most of the Indo-Pacific region. However, decadal HSSL patterns explain 10–20% of DSL variance in the south tropical Pacific, the subtropical Pacific, and offshore the US west coast. The HSSL trends are an integral part of DSL trends in

Table 2. Linear Trends of the Mass Sea Level Component (mm yr^{-1}) Averaged in the North Pacific, the South Pacific, and the Global Ocean Over Given Periods[a]

	1996–2006		2003–2011		2003–2013
	P2014 Residue Method	ECCO	GRACE Mascon	ECCO	P2014 GRACE Harmonic
North Pacific	$+1.53 \pm 0.58$	$+2.68 \pm 0.29$	$+3.23 \pm 0.36$	$+2.66 \pm 0.32$	$+3.59 \pm 0.71$
South Pacific	$+1.03 \pm 0.40$	$+2.29 \pm 0.35$	-0.51 ± 0.52	$+2.16 \pm 0.42$	$+0.08 \pm 0.62$
Global mean	$+1.47 \pm 0.45$	$+2.16 \pm 0.17$	$+1.09 \pm 0.18$	$+2.18 \pm 0.25$	$+1.53 \pm 0.36$

[a]Results of the residue method and the GRACE harmonic are cited directly from *Purkey et al.* [2014]. Results of ECCO and the GRACE mascon are calculated from this study. Uncertainties of the ECCO and GRACE mascon results denote the 95% confidence interval based on the two-sided Student's *t* test. The seasonal cycle is removed before calculating the linear trend. The North and South Pacific are defined as 150°E–130°W, 0°N–50°N, and 150°E–70°W, 0°S–50°S, respectively. Note that global mean is retained here to be consistent with *Purkey et al.* [2014].

the northeast subtropical Pacific. The compensation between TSSL and HSSL is identified for the decadal variability and the trend in the Pacific Ocean. ECCO, but not ESTOC, indicates 2–3 mm yr^{-1} HSSL rises in the south subtropical Pacific, and a similar rate of HSSL falls in the far northwest Pacific, counteracting the TSSL trends in those regions. Temperature responses associated with the interannual and decadal TSSL fingerprints show extrema at around 100 m depth, especially in the tropics. Salinity responses associated with the HSSL fingerprints, in contrast, tend to be surface intensified. The decadal temperature and salinity signals are capable of penetrating into greater depths in some regions compared to the interannual signals.

The MassSL interannual and decadal fingerprints each explains about 30% of DSL variance around Australia and on the shelves of the Asian marginal seas [also see *Wang et al.*, 2015]. In the open oceans, the MassSL fingerprints are mostly weak (<5 mm), with significant signals only identified in the far North and Southeast Pacific on interannual time scale, accounting for 5–10% of DSL variance [also see *Ponte and Piecuch*, 2014]. The dominant role of wind stress curl in modulating the interannual variability of MassSL in highlatitudes [*Boening et al.*, 2011] applies to both ECCO and ESTOC. The ECCO and ESTOC MassSL standard deviation patterns are in a good agreement with the GRACE mascon solution, but the MassSL linear trend patterns are less consistent in the various estimates. In particular, the hemispherically asymmetric trend patterns found in the two GRACE solutions are absent in both ECCO and ESTOC. In addition, ECCO features about

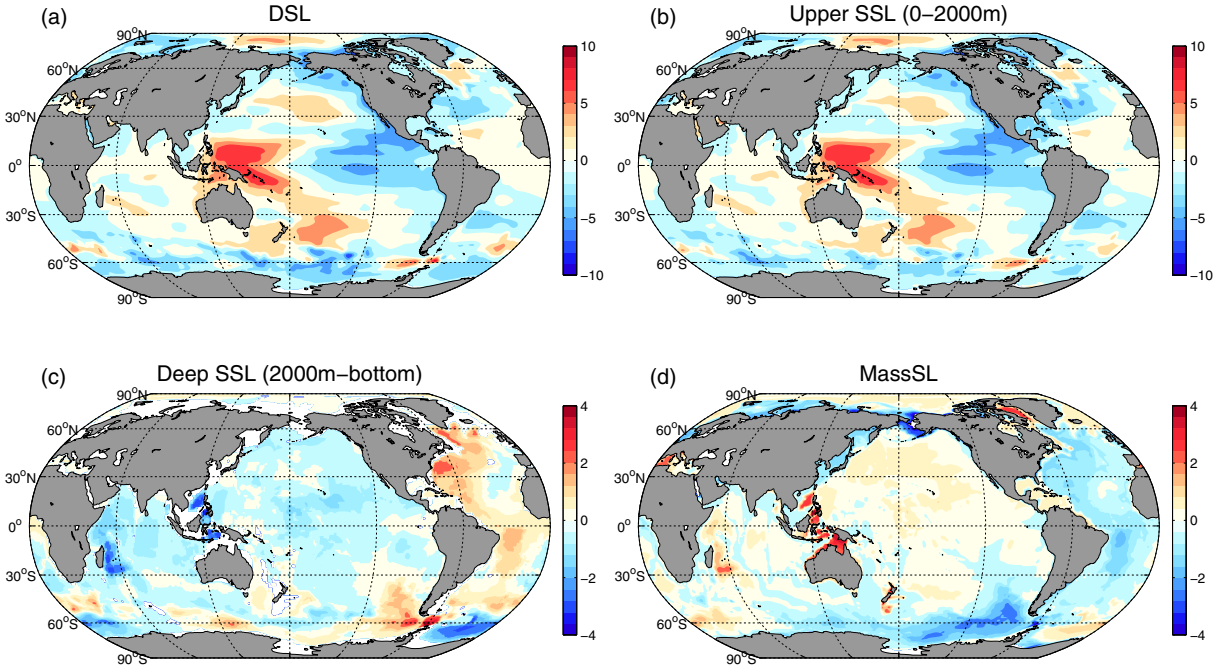

Figure 13. Linear trends over 1992–2011 (mm yr^{-1}) of (a) dynamic sea level (DSL), (b) steric sea level integrated between 0 and 2000 m (upper SSL), (c) steric sea level integrated from 2000 m to the seafloor (deep SSL), and mass sea level (MassSL). Results are based on ECCO with global means removed. Note that the bottom panels have a reduced color range.

2 mm yr^{-1} MassSL rises in several deep basins (depth >3000 m), and MassSL falls at about 1 mm yr^{-1} over some shelf seas. But those patterns cannot be observed in ESTOC.

One might wonder if a multivariate regression model using additional climate indices, such as the Southern Annular mode (SAM) [*Gong and Wang*, 1999], the North Pacific Gyre Oscillation (NPGO) [*Di Lorenzo et al*., 2008], and the Indian Ocean Dipole (IOD) [*Saji et al*., 1999], could better resolve sea level variability and change than the one used here. *Palanisamy et al*. [2015a] found that after removing the IPO-related signals, the leading EOF of residual signals resembles ENSO Modoki patterns in the Pacific Ocean, and accounts for 6% of the variance. *Frankcombe et al*. [2015] showed that by adding the indices of the IOD and SAM to the regression model used here, an additional 5% of sea level variance over the Indo-Pacific region was resolved. These improvements are marginal compared to around 40% variance explained in this study (Figure 1); hence, they are unlikely to significantly change our main results.

Purkey et al. [2014, hereinafter P2014] estimated the spatial-mean linear trend of MassSL for the North Pacific, the South Pacific, and the global ocean using observations (defined as the residue method in P2014) and the GRACE harmonic solution. Here we compare their results with that derived from ECCO and the GRACE mascon solution (Table 2). To be consistent with P2014, the global mean MassSL is kept for ECCO and the GRACE mascon. The global averaged atmospheric pressure is removed for the GRACE mascon using the ERA-Interm reanalysis [*Dee et al*., 2011]. It only contributed an insignificant linear trend of $+0.04 \pm 0.16$ mm yr^{-1} over 2003–2011. During 1996–2006, the global mean trend is $+1.47 \pm 0.45$ mm yr^{-1} from P2014 (residue method), but it is $+2.16 \pm 0.17$ mm yr^{-1} in ECCO. During the same period, the North Pacific trend is different from the global mean value with a marginal significance in ECCO, but the two trends are not significantly different from each other in P2014 (Table 2). Over 2003–2011, the results of the GRACE harmonic (from P2014) and the GRACE mascon are consistent with each other within their uncertainties (Table 2). Nonetheless, differences between the GRACE and the ECCO results are evident during the same period. First, the global mean trend from the GRACE mascon ($+1.09 \pm 0.18$ mm yr^{-1}) is a factor of 2 smaller than ECCO's estimate ($+2.18 \pm 0.25$ mm yr^{-1}). Second, the North Pacific trend is 3 times larger than the global mean trend in the GRACE mascon, but the two trends are similar in ECCO (Table 2). Clearly above comparisons highlight an urgent need to reconcile the maps of the MassSL linear trend from various data sets in future studies.

Landerer et al. [2007] suggested a simple redistribution model in which the warming (cooling) of deep ocean leads to ocean mass being redistributed into shallow (deep) regions. A similar conclusion is drawn in *Piecuch et al*. [2015a] by a perturbation experiment with geothermal fluxes. In addition to their studies, we identify a significant spatial correlation of the trend map between MassSL and deep SSL (integrated from the seafloor to 2000 m) in ECCO at -0.76 ± 0.10 over the Indo-Pacific region and -0.69 ± 0.06 for the global ocean (Figure 13). Those results imply that a long-term change in deep ocean states (e.g., warming or cooling below 2000 m) has an impact on long-term mass redistribution patterns. Future studies are required to quantify the relative importance of the deep ocean states along with surface buoyancy fluxes, geothermal fluxes [*Piecuch et al*., 2015a], and wind stress [*Johnson and Chambers*, 2013] in controlling MassSL long-term redistribution patterns.

Acknowledgments
We would like to thank Estimating the Circulation & Climate of the Ocean (ECCO) Consortium for providing the ECCO.v4.r2 product that can be downloaded from ftp://mit.ecco-group.org/ecco_for_las/version_4/release2/. GRACE ocean data were processed by Don P. Chambers, supported by the NASA MEaSUREs Program, and are available at http://grace.jpl.nasa.gov. GRACE CSR mascon solution was downloaded from http://www.csr.utexas.edu/grace. We also thank Shuhei Masuda for providing ESTOC data and comments on our analyses of ESTOC data. Detailed comments and constructive suggestions from Didier Monselesan are acknowledged. J.A.C. and X.Z. were supported by the Australian Climate Change Science Program (ACCSP), and X.Z. was also supported by the National Environmental Science Programme (NESP). J.H. and Q.W. were supported by the National Basic Research Program of China (2015CB954004). Q.W.'s visiting at CSIRO was funded by the China Scholarship Council (201506310098).

References

Antonov, J. I., S. Levitus, and T. P. Boyer (2002), Steric sea level variations during 1957-1994: Importance of salinity, *J. Geophys. Res.*, *107*(C12), 8013, doi:10.1029/2001JC000964.

Becker, M., B. Meyssignac, C. Letetrel, W. Llovel, A. Cazenave, and T. Delcroix (2012), Sea level variations at tropical Pacific islands since 1950, *Global Planet. Change*, *80 81–*, 85–98, doi:10.1016/j.gloplacha.2011.09.004.

Boening, C., T. Lee, and V. Zlotnicki (2011), A record-high ocean bottom pressure in the South Pacific observed by GRACE, *Geophys. Res. Lett.*, *38*, L04602, doi:10.1029/2010GL046013.

Bromirski, P. D., A. J. Miller, R. E. Flick, and G. Auad (2011), Dynamical suppression of sea level rise along the Pacific coast of North America: Indications for imminent acceleration, *J. Geophys. Res.*, *116*, C07005, doi:10.1029/2010JC006759.

Cai, W. (2005), Transmission of ENSO signal to the Indian Ocean, *Geophys. Res. Lett.*, *32*, L05616, doi:10.1029/2004GL021736.

Cazenave, A., and W. Llovel (2010), Contemporary sea level rise, *Ann. Rev. Mar. Sci.*, *2*(1), 145–173, doi:10.1146/annurev-marine-120308-081105.

Cazenave, A., and F. Remy (2011), Sea level and climate: Measurements and causes of changes, *WIREs Clim. Change*, *2*(5), 647–662, doi:10.1002/wcc.139.

Chambers, D. P. (2011), ENSO-correlated fluctuations in ocean bottom pressure and wind-stress curl in the North Pacific, *Ocean Sci.*, *7*(5), 685–692, doi:10.5194/os-7-685-2011.

Chambers, D. P., and J. A. Bonin (2012), Evaluation of Release-05 GRACE time-variable gravity coefficients over the ocean, *Ocean Sci.*, *8*(5), 859–868, doi:10.5194/os-8-859-2012.

Chambers, D. P., B. D. Tapley, and R. H. Stewart (1999), Anomalous warming in the Indian Ocean coincident with El Niño, *J. Geophys. Res.*, *104*(C2), 3035–3047, doi:10.1029/1998JC900085.
Chen, X., and J. M. Wallace (2015), ENSO-like variability: 1900–2013, *J. Clim.*, *28*(24), 9623–9641, doi:10.1175/JCLI-D-15-0322.1.
Cheng, X., L. Li, Y. Du, J. Wang, and R.-X. Huang (2013), Mass-induced sea level change in the northwestern North Pacific and its contribution to total sea level change, *Geophys. Res. Lett.*, *40*, 3975–3980, doi:10.1002/grl.50748.
Church, J. A., and N. J. White (2011), Sea-level rise from the late 19th to the early 21st century, *Surv. Geophys.*, *32*(4–5), 585–602, doi:10.1007/s10712-011-9119-1.
Church, J. A., et al. (2013), Sea level change, in *Climate Change 2013: The Physical Science Basis. Contribution of Working Group I to the Fifth Assessment Report of the Intergovernmental Panel on Climate Change*, edited by T. F. Stocker et al., pp. 1137–1216, Cambridge Univ. Press, Cambridge, U. K.
Davis, R. E. (1976), Predictability of sea surface temperature and sea level pressure anomalies over the North Pacific Ocean, *J. Phys. Oceanogr.*, *6*(3), 249–266, doi:10.1175/1520-0485(1976)006 < 0249:POSSTA>2.0.CO;2.
Dee, D. P., et al. (2011), The ERA-Interim reanalysis: Configuration and performance of the data assimilation system, *Q. J. R. Meteorol. Soc.*, *137*(656), 553–597, doi:10.1002/qj.828.
Delcroix, T., and C. Hénin (1991), Seasonal and interannual variations of sea surface salinity in the tropical Pacific Ocean, *J. Geophys. Res.*, *96*(C12), 22,135–22,150, doi:10.1029/91JC02124.
Delcroix, T., and M. McPhaden (2002), Interannual sea surface salinity and temperature changes in the western Pacific warm pool during 1992-2000, *J. Geophys. Res.*, *107*(C12), 8002, doi:10.1029/2001JC000862.
Deser, C., M. A. Alexander, S.-P. Xie, and A. S. Phillips (2010), Sea surface temperature variability: Patterns and mechanisms, *Ann. Rev. Mar. Sci.*, *2*(1), 115–143, doi:10.1146/annurev-marine-120408-151453.
Durack, P. J., S. E. Wijffels, and P. J. Gleckler (2014), Long-term sea-level change revisited: The role of salinity, *Environ. Res. Lett.*, *9*(11), 114017, doi:10.1088/1748-9326/9/11/114017.
Emery, W. J., and R. E. Thomson (2001), *Data Analysis Methods in Physical Oceanography*, Elsevier, Amsterdam.
Enfield, D. B., and J. S. Allen (1980), On the structure and dynamics of monthly mean sea level anomalies along the Pacific Coast of North and South America, *J. Phys. Oceanogr.*, *10*(4), 557–578, doi:10.1175/1520-0485(1980)010 < 0557:OTSADO>2.0.CO;2.
Feng, M. (2004), Multidecadal variations of Fremantle sea level: Footprint of climate variability in the tropical Pacific, *Geophys. Res. Lett.*, *31*, L16302, doi:10.1029/2004GL019947.
Feng, M., and G. Meyers (2003), Interannual variability in the tropical Indian Ocean: A two-year time-scale of Indian Ocean Dipole, *Deep Sea Res., Part II*, *50*(12–13), 2263–2284, doi:10.1016/S0967-0645(03)00056-0.
Feng, M., M. J. McPhaden, and T. Lee (2010), Decadal variability of the Pacific subtropical cells and their influence on the southeast Indian Ocean, *Geophys. Res. Lett.*, *37*, L09606, doi:10.1029/2010GL042796.
Feng, M., C. Böning, A. Biastoch, E. Behrens, E. Weller, and Y. Masumoto (2011), The reversal of the multi-decadal trends of the equatorial Pacific easterly winds, and the Indonesian Throughflow and Leeuwin Current transports, *Geophys. Res. Lett.*, *38*, L11604, doi:10.1029/2011GL047291.
Forget, G., and R. M. Ponte (2015), The partition of regional sea level variability, *Prog. Oceanogr.*, *137*, 173–195, doi:10.1016/j.pocean.2015.06.002.
Forget, G., J.-M. Campin, P. Heimbach, C. N. Hill, R. M. Ponte, and C. Wunsch (2015), ECCO version 4: An integrated framework for non-linear inverse modeling and global ocean state estimation, *Geosci. Model Dev.*, *8*(10), 3071–3104, doi:10.5194/gmd-8-3071-2015.
Forget, G., J.-M. Campin, P. Heimbach, C. N. Hill, R. M. Ponte, and C. Wunsch (2016), ECCO version 4: Second release. [Available at http://hdl.handle.net/1721.1/102062.]
Frankcombe, L. M., S. McGregor, and M. H. England (2015), Robustness of the modes of Indo-Pacific sea level variability, *Clim. Dyn.*, *45*(5–6), 1281–1298, doi:10.1007/s00382-014-2377-0.
Gill, A. E., and P. P. Niller (1973), The theory of the seasonal variability in the ocean, *Deep Sea Res. Oceanogr. Abstr.*, *20*(2), 141–177, doi:10.1016/0011-7471(73)90049-1.
Gong, D., and S. Wang (1999), Definition of Antarctic Oscillation index, *Geophys. Res. Lett.*, *26*(4), 459–462, doi:10.1029/1999GL900003.
Hamlington, B. D., M. W. Strassburg, R. R. Leben, W. Han, R. S. Nerem, and K.-Y. Kim (2014), Uncovering an anthropogenic sea-level rise signal in the Pacific Ocean, *Nat. Clim. Change*, *4*(9), 782–785, doi:10.1038/nclimate2307.
Hamlington, B. D., R. R. Leben, K.-Y. Kim, R. S. Nerem, L. P. Atkinson, and P. R. Thompson (2015), The effect of the El Niño-Southern Oscillation on U.S. regional and coastal sea level, *J. Geophys. Res. Ocean.*, *120*, 3970–3986, doi:10.1002/2014JC010602.
Jin, F.-F. (1997), An equatorial ocean recharge paradigm for ENSO. Part I: Conceptual model, *J. Atmos. Sci.*, *54*(7), 811–829, doi:10.1175/1520-0469(1997)054 < 0811:AEORPF>2.0.CO;2.
Johnson, G. C., and D. P. Chambers (2013), Ocean bottom pressure seasonal cycles and decadal trends from GRACE Release-05: Ocean circulation implications, *J. Geophys. Res. Ocean.*, *118*, 4228–4240, doi:10.1002/jgrc.20307.
Köhl, A. (2014), Detecting processes contributing to interannual halosteric and thermosteric sea level variability, *J. Clim.*, *27*(6), 2417–2426, doi:10.1175/JCLI-D-13-00412.1.
Landerer, F. W., J. H. Jungclaus, and J. Marotzke (2007), Ocean bottom pressure changes lead to a decreasing length-of-day in a warming climate, *Geophys. Res. Lett.*, *34*, L06307, doi:10.1029/2006GL029106.
Landerer, F. W., J. H. Jungclaus, and J. Marotzke (2008), El Niño–Southern Oscillation signals in sea level, surface mass redistribution, and degree-two geoid coefficients, *J. Geophys. Res.*, *113*, C08014, doi:10.1029/2008JC004767.
Lee, T., and M. J. McPhaden (2008), Decadal phase change in large-scale sea level and winds in the Indo-Pacific region at the end of the 20th century, *Geophys. Res. Lett.*, *35*, L01605, doi:10.1029/2007GL032419.
Levitus, S., J. I. Antonov, T. P. Boyer, H. E. Garcia, and R. A. Locarnini (2005), Linear trends of zonally averaged thermosteric, halosteric, and total steric sea level for individual ocean basins and the world ocean, (1955–1959)–(1994–1998), *Geophys. Res. Lett.*, *32*, L16601, doi:10.1029/2005GL023761.
Li, Y., and W. Han (2015), Decadal sea level variations in the Indian Ocean investigated with HYCOM: Roles of climate modes, ocean internal variability, and stochastic wind forcing, *J. Clim.*, *28*(23), 9143–9165, doi:10.1175/JCLI-D-15-0252.1.
Llovel, W., and T. Lee (2015), Importance and origin of halosteric contribution to sea level change in the southeast Indian Ocean during 2005-2013, *Geophys. Res. Lett.*, *42*, 1148–1157, doi:10.1002/2014GL062611.
Lombard, A., G. Garric, and T. Penduff (2009), Regional patterns of observed sea level change: Insights from a 1/4° global ocean/sea-ice hindcast, *Ocean Dyn.*, *59*(3), 433–449, doi:10.1007/s10236-008-0161-6.
Di Lorenzo, E., et al. (2008), North Pacific Gyre Oscillation links ocean climate and ecosystem change, *Geophys. Res. Lett.*, *35*, L08607, doi:10.1029/2007GL032838.
Lyu, K., X. Zhang, J. A. Church, and J. Hu (2015), Evaluation of the interdecadal variability of sea surface temperature and sea level in the Pacific in CMIP3 and CMIP5 models, *Int. J. Climatol.*, *36*, 3723–3740, doi:10.1002/joc.4587.

Mantua, N. J., and S. R. Hare (2002), The Pacific Decadal Oscillation, *J. Oceanogr.*, *58*(1), 35–44, doi:10.1023/A:1015820616384.
Marshall, J., A. Adcroft, C. Hill, L. Perelman, and C. Heisey (1997), A finite-volume, incompressible Navier Stokes model for studies of the ocean on parallel computers, *J. Geophys. Res.*, *102*(C3), 5753–5766, doi:10.1029/96JC02775.
McCreary, J. P., and P. Lu (1994), Interaction between the subtropical and equatorial ocean circulations: The subtropical cell, *J. Phys. Oceanogr.*, *24*(2), 466–497, doi:10.1175/1520-0485(1994)024 < 0466:IBTSAE>2.0.CO;2.
Meinen, C. S., and M. J. McPhaden (2000), Observations of warm water volume changes in the equatorial Pacific and their relationship to El Niño and La Niña, *J. Clim.*, *13*(20), 3551–3559, doi:10.1175/1520-0442(2000)013 < 3551:OOWWVC>2.0.CO;2.
Merrifield, M. A. (2011), A shift in western tropical Pacific sea level trends during the 1990s, *J. Clim.*, *24*(15), 4126–4138, doi:10.1175/2011JCLI3932.1.
Merrifield, M. A., P. R. Thompson, and M. Lander (2012), Multidecadal sea level anomalies and trends in the western tropical Pacific, *Geophys. Res. Lett.*, *39*, L13602, doi:10.1029/2012GL052032.
Moon, J.-H., Y. T. Song, P. D. Bromirski, and A. J. Miller (2013), Multidecadal regional sea level shifts in the Pacific over 1958-2008, *J. Geophys. Res. Oceans*, *118*, 7024–7035, doi:10.1002/2013JC009297.
Moon, J.-H., Y. T. Song, and H. Lee (2015), PDO and ENSO modulations intensified decadal sea level variability in the tropical Pacific, *J. Geophys. Res. Oceans*, *120*, 8229–8237, doi:10.1002/2015JC011139.
Nerem, R. S., D. P. Chambers, E. W. Leuliette, G. T. Mitchum, and B. S. Giese (1999), Variations in global mean sea level associated with the 1997-1998 ENSO event: Implications for measuring long term sea level change, *Geophys. Res. Lett.*, *26*(19), 3005–3008, doi:10.1029/1999GL002311.
Nidheesh, A. G., M. Lengaigne, J. Vialard, A. S. Unnikrishnan, and H. Dayan (2013), Decadal and long-term sea level variability in the tropical Indo-Pacific Ocean, *Clim. Dyn.*, *41*(2), 381–402, doi:10.1007/s00382-012-1463-4.
Osafune, S., S. Masuda, N. Sugiura, and T. Doi (2015), Evaluation of the applicability of the estimated state of the global ocean for climate research (ESTOC) data set, *Geophys. Res. Lett.*, *42*, 4903–4911, doi:10.1002/2015GL064538.
Pacanowski, R., and S. M. Griffies (2000), *MOM 3.0 Manual*, Geophys. Fluid Dyn. Lab., Natl. Atmos. Admin., Princeton, N. J.
Palanisamy, H., B. Meyssignac, A. Cazenave, and T. Delcroix (2015a), Is anthropogenic sea level fingerprint already detectable in the Pacific Ocean?, *Environ. Res. Lett.*, *10*(8), 84024, doi:10.1088/1748-9326/10/8/084024.
Palanisamy, H., A. Cazenave, T. Delcroix, and B. Meyssignac (2015b), Spatial trend patterns in the Pacific Ocean sea level during the altimetry era: The contribution of thermocline depth change and internal climate variability, *Ocean Dyn.*, *65*(3), 341–356, doi:10.1007/s10236-014-0805-7.
Piecuch, C. G., and R. M. Ponte (2011), Mechanisms of interannual steric sea level variability, *Geophys. Res. Lett.*, *38*, L15605, doi:10.1029/2011GL048440.
Piecuch, C. G., and R. M. Ponte (2012), Buoyancy-driven interannual sea level changes in the southeast tropical Pacific, *Geophys. Res. Lett.*, *39*, L05607, doi:10.1029/2012GL051130.
Piecuch, C. G., K. J. Quinn, and R. M. Ponte (2013), Satellite-derived interannual ocean bottom pressure variability and its relation to sea level, *Geophys. Res. Lett.*, *40*, 3106–3110, doi:10.1002/grl.50549.
Piecuch, C. G., P. Heimbach, R. M. Ponte, and G. Forget (2015a), Sensitivity of contemporary sea level trends in a global ocean state estimate to effects of geothermal fluxes, *Ocean Modell.*, *96*, 214–220, doi:10.1016/j.ocemod.2015.10.008.
Piecuch, C. G., I. Fukumori, R. M. Ponte, and O. Wang (2015b), Vertical structure of ocean pressure variations with application to satellite-gravimetric observations, *J. Atmos. Oceanic Technol.*, *32*(3), 603–613, doi:10.1175/JTECH-D-14-00156.1.
Ponte, R. M., and C. G. Piecuch (2014), Interannual bottom pressure signals in the Australian–Antarctic and Bellingshausen Basins, *J. Phys. Oceanogr.*, *44*(5), 1456–1465, doi:10.1175/JPO-D-13-0223.1.
Purkey, S. G., G. C. Johnson, and D. P. Chambers (2014), Relative contributions of ocean mass and deep steric changes to sea level rise between 1993 and 2013, *J. Geophys. Res. Oceans*, *119*, 7509–7522, doi:10.1002/2014JC010180.
Qiu, B., and S. Chen (2006), Decadal variability in the large-scale sea surface height field of the South Pacific Ocean: Observations and causes, *J. Phys. Oceanogr.*, *36*(9), 1751–1762, doi:10.1175/JPO2943.1.
Qiu, B., and S. Chen (2012), Multidecadal sea level and gyre circulation variability in the northwestern tropical Pacific Ocean, *J. Phys. Oceanogr.*, *42*(1), 193–206, doi:10.1175/JPO-D-11-061.1.
Roemmich, D., and J. Gilson (2011), The global ocean imprint of ENSO, *Geophys. Res. Lett.*, *38*, L13606, doi:10.1029/2011GL047992.
Roemmich, D., J. Church, J. Gilson, D. Monselesan, P. Sutton, and S. Wijffels (2015), Unabated planetary warming and its ocean structure since 2006, *Nat. Clim. Change*, *5*(3), 240–245, doi:10.1038/nclimate2513.
Roemmich, D., J. Gilson, P. Sutton, and N. Zilberman (2016), Multidecadal change of the South Pacific gyre circulation, *J. Phys. Oceanogr.*, *46*(6), 1871–1883, doi:10.1175/JPO-D-15-0237.1.
Saji, N. H., B. N. Goswami, P. N. Vinayachandran, and T. Yamagata (1999), A dipole mode in the tropical Indian Ocean, *Nature*, *401*(6751), 360–363, doi:10.1038/43854.
Save, H., S. Bettadpur, and B. D. Tapley (2016), High resolution CSR GRACE RL05 mascons, *J. Geophys. Res. Solid Earth*, *121*, 7547–7569, doi:10.1002/2016JB013007.
Schwarzkopf, F. U., and C. W. Böning (2011), Contribution of Pacific wind stress to multi-decadal variations in upper-ocean heat content and sea level in the tropical south Indian Ocean, *Geophys. Res. Lett.*, *38*, L12602, doi:10.1029/2011GL047651.
Song, Y. T., and V. Zlotnicki (2008), Subpolar ocean bottom pressure oscillation and its links to the tropical ENSO, *Int. J. Remote Sens.*, *29*(21), 6091–6107, doi:10.1080/01431160802175538.
Stammer, D., A. Cazenave, R. M. Ponte, and M. E. Tamisiea (2013), Causes for contemporary regional sea level changes, *Ann. Rev. Mar. Sci.*, *5*(1), 21–46, doi:10.1146/annurev-marine-121211-172406.
Thacker, W. C., and R. B. Long (1988), Fitting dynamics to data, *J. Geophys. Res.*, *93*(C2), 1227–1240, doi:10.1029/JC093iC02p01227.
Trenary, L. L., and W. Han (2012), Intraseasonal-to-interannual variability of South Indian Ocean sea level and thermocline: Remote versus local forcing, *J. Phys. Oceanogr.*, *42*(4), 602–627, doi:10.1175/JPO-D-11-084.1.
Wang, J., J. Wang, and X. Cheng (2015), Mass-induced sea level variations in the Gulf of Carpentaria, *J. Oceanogr.*, *71*(4), 449–461, doi:10.1007/s10872-015-0304-6.
Watkins, M. M., D. N. Wiese, D.-N. Yuan, C. Boening, and F. W. Landerer (2015), Improved methods for observing Earth's time variable mass distribution with GRACE using spherical cap mascons, *J. Geophys. Res. Solid Earth*, *120*, 2648–2671, doi:10.1002/2014JB011547.
Wijffels, S., and G. Meyers (2004), An intersection of oceanic waveguides: Variability in the Indonesian Throughflow region, *J. Phys. Oceanogr.*, *34*(5), 1232–1253, doi:10.1175/1520-0485(2004)034 < 1232:AIOOWV>2.0.CO;2.

Zhang, L., and T. Qu (2014), Low-frequency variability of South Pacific Tropical Water from Argo, *Geophys. Res. Lett.*, *41*, 2441–2446, doi: 10.1002/2014GL059490.
Zhang, L., and T. Qu (2015), Low-frequency variability of the south Pacific subtropical gyre as seen from satellite altimetry and Argo, *J. Phys. Oceanogr.*, *45*(12), 3083–3098, doi:10.1175/JPO-D-15-0026.1.
Zhang, X., and J. A. Church (2012), Sea level trends, interannual and decadal variability in the Pacific Ocean, *Geophys. Res. Lett.*, *39*, L21701, doi:10.1029/2012GL053240.